Theory of sorption hysteresis in nanoporous solids: Part I Snap-through instabilities

Zdeněk P. Bažant [a],*, Martin Z. Bazant [b]

[a] McCormick School, Civil Engineering and Materials Science, Northwestern University, 2145 Sheridan Road, CEE/A135, Evanston, IL 60208, United States
[b] Chemical Engineering and Mathematics, Massachusetts Institute of Technology, Cambridge, MA 02139, United States

ARTICLE INFO

ABSTRACT

The sorption–desorption hysteresis observed in many nanoporous solids, at vapor pressures low enough for the liquid (capillary) phase of the adsorbate to be absent, has long been vaguely attributed to some sort of 'pore collapse'. However, the pore collapse has never been documented experimentally and explained mathematically. The present work takes an analytical approach to account for discrete molecular forces in the nanopore fluid and proposes two related mechanisms that can explain the hysteresis at low vapor pressure without assuming any pore collapse nor partial damage to the nanopore structure. The first mechanism, presented in Part I, consists of a series of snap-through instabilities during the filling or emptying of non-uniform nanopores or nanoscale asperities. The instabilities are caused by non-uniqueness in the misfit disjoining pressures engendered by a difference between the nanopore width and an integer multiple of the thickness of a monomolecular adsorption layer. The wider the pore, the weaker the mechanism, and it ceases to operate for pores wider than about 3 nm. The second mechanism, presented in Part II, consists of molecular coalescence, or capillary condensation, within a partially filled surface, nanopore or nanopore network. This general thermodynamic instability is driven by attractive intermolecular forces within the adsorbate and forms the basis for developing a unified theory of both mechanisms. The ultimate goals of the theory are to predict the fluid transport in nanoporous solids from microscopic first principles, determine the pore size distribution and internal surface area from sorption tests, and provide a way to calculate the disjoining pressures in filled nanopores, which play an important role in the theory of creep and shrinkage.

© 2012 Published by Elsevier Ltd.

1. Introduction

The sorption isotherm, characterizing the isothermal dependence of the adsorbate mass content on the relative vapor pressure at thermodynamic equilibrium, is a basic characteristic of adsorbent porous solids. It is important for estimating the internal pore surface of hydrated Portland cement paste and other materials. It represents the essential input for solutions of the diffusion equation for drying and wetting of concrete, for calculations of the release of methane from coal deposits and rock masses, for the analysis of sequestration of carbon dioxide in rock formations, etc. Its measurements
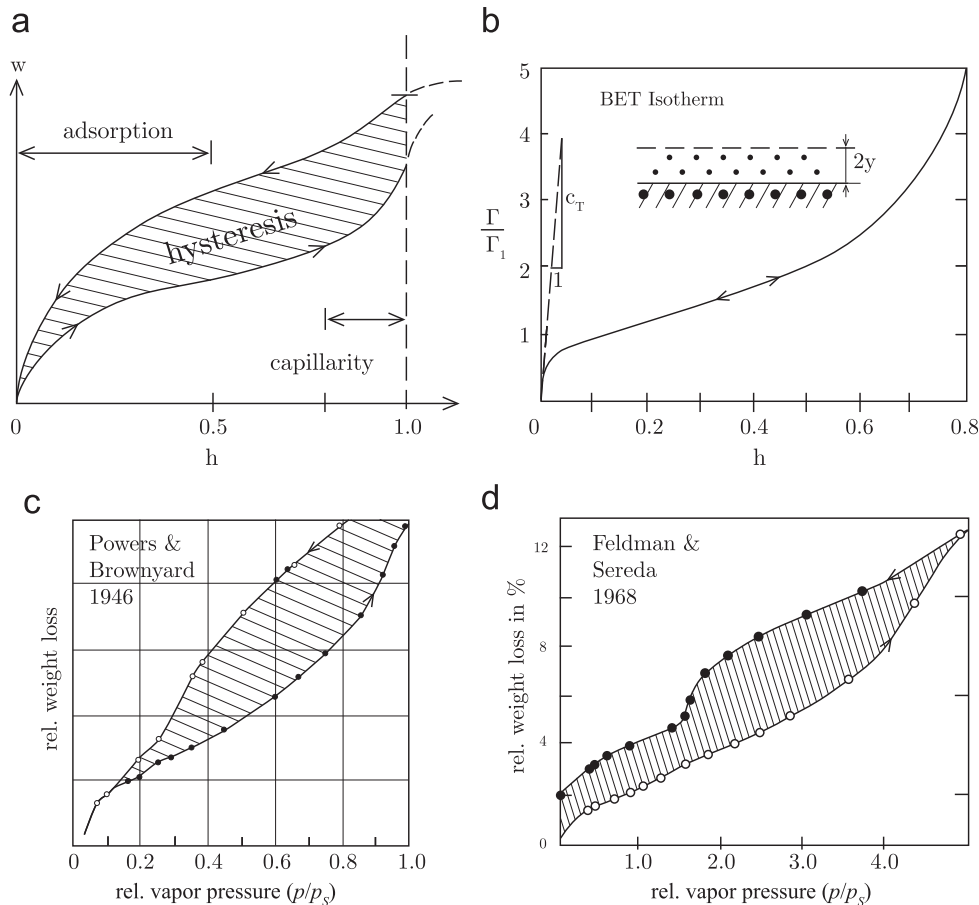

Fig. 1. (a) Typical desorption and sorption isotherms; (b) BET isotherm; (c) and (d) desorption and sorption isotherms measured on hardened Portland cement paste.

provide vital information for determining the internal surface of nanoporous solids (Powers and Brownyard, 1946; Adolphs and Setzer, 1996; Jennings, 2000; Adolphs et al., 2002; Espinosa and Franke, 2006; Baroghel-Bouny, 2007).

An important feature of sorption experiments with water, nitrogen, alcohol, methane, carbon dioxide, etc. has been a pronounced hysteresis, observed at both high and low vapor pressures and illustrated by two classical experiments in Fig. 1c and d; in Powers and Brownyard (1946, p. 277) and Feldman and Sereda (1964) (see also, e.g. Feldman and Sereda, 1968; Rarick et al., 1995; Adolphs et al., 2002; Espinosa and Franke, 2006; Baroghel-Bouny, 2007). For adsorbates that exist at room temperature in a liquid form, e.g. water, the room temperature hysteresis at high vapor pressures near saturation has easily been explained by non-uniqueness of the surfaces of capillary menisci of liquid adsorbate in larger pores (e.g., the 'ink-bottle' effect Brunauer, 1943).

However, a liquid (capillary) water can exist in the pores only if the capillary tension under the meniscus (which is given by the Kelvin–Laplace equation) does not exceed the tensile strength of liquid water, which is often thought to be exhausted at no less than 45% of the saturation pressure, if not much higher. Anyway, at vapor pressures less than about 80% of the saturation pressure, the liquid phase represents a small fraction of the total evaporable water content of calcium silicate hydrates (C–S–H) (Jennings, submitted for publication); see Fig. 1a.

For more than 60 years, the hysteresis in the range of low vapor pressures (lower than about 80% of saturation in the case of C–S–H) has remained a perplexing and unexplained feature. In that range, most or all of the adsorbate is held by surface adsorption. The gases and porous solids of interest generally form adsorption layers consisting of several monomolecular layers (Fig. 1b). The multi-layer adsorption is described by the BET isotherm (Brunauer et al., 1938) (Fig. 1b), which is reversible. Sorption experiments have generally been interpreted under the (tacit) hypothesis of free adsorption, i.e., the adsorption in which the surface of the adsorption layer is exposed to gas.

In nanoporous solids, though, most of the adsorbate is in the form of hindered adsorption layers, i.e., layers confined in the nanopores which are sometimes defined as pores ≤ 2 nm wide (Balbuena et al., 1993). For instance, 1 cm^3 of hardened Portland cement paste contains the internal surface of about 500 m^2. The total porosity is typically about 50%, with the large capillary pores occupying about 15% and the nanopores about 35% of the material volume. So, the average width of nanopores is about 0.35 cm^3/500 m$^2 = 0.7$ nm, which is about three water molecular diameters. The hindered adsorbed layers in such nanopores have no surface directly exposed to vapor and communicate with the vapor in macropores by diffusion along the layer. It has been well known that a large transverse stress, called the disjoining pressure (Derjaguin, 1940) (or solvation pressure Balbuena et al., 1993), must develop in these layers.

Development of the theory of hindered adsorption for concrete was stimulated by Powers' general ideas of the creep mechanism (Powers, 1966). Its mathematical formulation for C–S–H gradually emerged in Bažant (1970a, 1970b, 1972a, 1972b), and was reviewed in a broad context in Bažant (1975). But this theory of hindered adsorption is also reversible. Thus, although a theory exists, it cannot explain the hysteresis.

The sorption hysteresis in hardened Portland cement paste, concrete and various solid gels (Scherer, 1999; Jennings et al., 2008) has for decades been vaguely attributed to some sort of changes of the nanopore structure. In particular, it was proposed that the exit of water, called the interlayer water, from the narrowest nanopores would somehow cause the pores to collapse (Feldman and Sereda, 1968; Espinosa and Franke, 2006; Baroghel-Bouny, 2007; Thomas et al., 2008) (see Rarick et al., 1995, Figs. 13 and 16, Espinosa and Franke, 2006, Fig. 1, or Jennings, submitted for publication, Fig. 9), picturing hypothesized pore width changes of the order of 100%.

However, if a mathematical model of such a mechanism is attempted, it inevitably predicts enormous macroscopic deformations, far larger than the observed shrinkage caused by drying. For example, measurements on the hardened cement paste reveal desorption and sorption isotherms (Fig. 1) in which the water contents w for the same humidity h differ by 50% or more. As before, consider that the nanopores represent 35% of the total volume of material. Thus, if the 50% difference in w were totally due to collapsing nanopores, the relative volume change in the material would have to be about $0.35 \times 0.50 = 0.175$. This means that the pore collapse would have to cause a linear shrinkage of about $0.175/3 \approx 6\%$. But the typical drying shrinkage of hardened cement pastes is one to two orders-of-magnitude smaller. Although the results of a more accurate analysis could differ by a factor of up to about 2, there is no way the hypothesis of pore collapse could be quantitatively reconciled with the shrinkage observations.

Another objection to the pore collapse hypothesis is that the isotherm for second desorption is much closer to that for first desorption than to that for first sorption. If this hypothesis was true, then the pores would have to get somehow reconstructed prior to the second desorption. So, the pore collapse hypothesis is untenable (and so is the use of this hypothesis for explaining the increase in creep of concrete due to simultaneous drying: Feldman and Sereda, 1968).

Another idea, qualitatively inferred from environmental scanning electron microscope studies (Hall et al., 1995), was to explain the hysteresis in cement pastes by new hydration of unreacted remnants of cement grains and the associated swelling which would be encroaching into the pore space and also causing pore wall damage. But how could one then explain that the second desorption isotherm is close to the first (Powers and Brownyard, 1946; Baroghel-Bouny, 2007)? Surely one cannot expect the grains to reversibly dehydrate during wetting sorption, and the pore wall damage to get repaired. Besides, in bulk, no measurable cement hydration takes place at pore humidities below about 0.70–0.85.

Here it will be shown that sorption hysteresis must occur even if the nanopore structure does not change. The main message of this work is that the number of molecular layers of adsorbate that can be confined in a nanopore is not unique, and that this non-uniqueness inevitably causes sorption hysteresis.

Non-uniqueness is also a salient feature of capillarity of liquid water in larger pores, typically of micrometer dimensions. In the capillary range, the non-uniqueness is classically explained by the afore-mentioned 'ink-bottle' effect, which exists even in two dimensions. In three dimensions, there is much broader range of topological and geometrical configurations which provide a richer and more potent source of non-uniqueness of liquid adsorbate content.

The simplest demonstration is a regular cubic array of identical spherical particles separated by a small gap δ between each pair. At $h=1$, either all the pore space can be filled by a liquid, or an anticlastic meniscus surface of a zero total curvature $r^{-1} = r_1^{-1} + r_2^{-1} = 0$ and of a liquid pressure equal to p_s can exist between each two spheres, with $r_1 = -r_2$ and $r_1, r_2 = $ principal curvature radii (the surface near the symmetry line of the pair of spheres is a rotational hyperbolic paraboloid). Such effects can explain 100% differences among equilibrium liquid contents w at $h=1$ observed in some experiments. It can even be shown that when both δ and r_1 (with $r_2 = -r_1$) approach zero in a certain way, then also the liquid content (as a continuum) approaches 0 (thus, in theory, an arbitrarily small but non-zero equilibrium liquid content at $h=1$ is possible, though extremely unlikely).

This three-dimensional picture, for example, explains why the non-uniqueness of sorption isotherm extends to $h > 1$ (as shown in Fig. 1a by dashed lines; here $h = p_v/p_s(T)$ is the relative vapor pressure, or relative humidity in the case of water, p_v is the pressure of vapor or gas; and $p_s(T)$ is the saturation vapor pressure). For $h > 1$, the vapor pressure $p_v > p_s$, the total curvature of the menisci is changed from positive to negative, the pores contain overpressurized vapor, and the hysteresis, or non-uniqueness, continues (Bažant and Thonguthai, 1978; Bažant and Kaplan, 1996). This non-uniqueness and hysteresis explains why the slope of the isotherm for $h > 1$ is one, or even two, orders of magnitude higher than one would calculate if all the water were liquid for $h > 1$ (in theory, this non-uniqueness can extend up to the critical point of water). In cements these phenomena are complicated by the fact that the chemical reactions of hydration withdraw some water from the pores, and create self-desiccation bubbles (thus one can practically never have concrete with no vapor, even for $p_v > p_s$).

The consequence of the non-uniqueness is that the sorption isotherm is not a function but a functional of the entire previous history of adsorbate content. Here we will show that the functional character extends to the range of hindered adsorption in nanopores.

The recent advent of molecular dynamic (MD) simulations is advancing the knowledge of nanoporous solids and gels or colloidal systems in a profound way (Pellenq et al., 2010; Coasne et al., 2008a, 2008b, 2009; Jönson et al., 2004, 2005; Smith et al., 2006; Malani et al., 2009; Vandamme et al., 2010). Particularly exciting have been the new results by Rolland Pellenq and co-workers at the Concrete Sustainability Hub (CSH) in MIT led by Franz-Josef Ulm (Bonnaud et al., 2010;

Brochard et al., 2011, 2012). These researchers used numerical MD simulations to study sorption and desorption in nanopores of coal and calcium silicate hydrates. Their MD simulations (Bonnaud et al., 2010, Figs. 3 and 4) demonstrated that the filling and emptying of pores 1 and 2 nm wide by water molecules exhibits marked hysteresis.

Especially revealing is the latest article of Pellenq et al. from MIT (Brochard et al., 2011). Simulating a chain of nanopores, they computed the distributions of disjoining (or transverse) pressure and found that it can alternate between negative (compressive) and positive (tensile), depending on the difference of pore width from an integer multiple of the natural thickness of an adsorbed monomolecular layer (see Brochard et al., 2011, Figs. 14 and 11). This discrete aspect of disjoining pressure, which cannot be captured by continuum thermodynamics, was a crucial finding of Pellenq et al. which stimulated the mathematical formulation of snap-through instabilities in Part I of this work. Oscillations between positive and negative disjoining pressures have also been revealed by density functional theory simulations of colloidal fluids or gels in Balbuena et al. (1993) (where the excess transverse stress is called the 'solvation pressure' rather than the disjoining pressure).

Nanoscale oscillations of the disjoining (or solvation) pressure have also been observed in the MD simulations of nitrogen molecules in rough slit-shaped carbon nanopores (using for carbon the quenched solid density functional theory) (Yang et al., 2011). It was concluded that the surface roughness damps these oscillations. This phenomenon may be important for the meso- or macroscale residual stresses and creep in C–S–H but, as argued here, not for the sorption isotherms that are dominated by dynamic snap-throughs.

This work is organized as follows. In Part I, we begin by summarizing the classical theory of multi-layer adsorption on free surfaces by Brunauer, Emmett and Teller (BET) (Brunauer et al., 1938), which is widely used to fit experimental data, but assumes reversible adsorption without any hysteresis. We then develop a general theory of hindered adsorption in nanopores which accounts for crucial and previously neglected effects of molecular discreteness as the pore width varies. This leads us to the first general mechanism for sorption hysteresis, snap-through instability in non-uniform pores, which is the focus of this Part I.

In Part II which follows (Bazant and Bažant), we show that the attractive forces between discrete adsorbed molecules can also lead to sorption hysteresis by molecular condensation in arbitrary nanopore geometries, including perfectly flat surfaces and pores. This second mechanism of hysteresis is a general thermodynamic instability of the homogeneous adsorbate that leads to stable high-density and low-density phases below the critical temperature. The mathematical formulation of Part II is thus based on non-equilibrium statistical mechanics. But here, in Part I, we begin to build the theory using more familiar models from solid mechanics and continuum thermodynamics.

2. Continuum thermodynamics of hindered adsorption in nanopores

Free adsorption: When a multi-molecular adsorption layer on a solid adsorbent surface is in contact with the gaseous phase of the adsorbate, the effective thickness a of the layer is well described by the BET equation (Brunauer et al., 1938, Eq. (28))

$$\Theta = \frac{a}{s_0} = \frac{\Gamma_w}{\Gamma_1} = \frac{1}{1-h} - \frac{1}{1-h+c_T h}, \quad c_T = c_0 e^{\Delta Q_a/RT} \tag{1}$$

where T is the absolute temperature, Γ_w is the mass of adsorbate per unit surface area; Γ_1 is the mass of one full molecular monolayer per unit area, Θ is the dimensionless surface coverage, h is the relative pressure of the vapor in macropores with which the adsorbed water is in thermodynamic equilibrium, R is the universal gas constant ($8314\ \mathrm{J\ kmole^{-1}\ K^{-1}}$), c_0 is the constant depending on the entropy of adsorption, ΔQ_a is the latent heat of adsorption minus latent heat of liquefaction, s_0 is the effective thickness of a monomolecular layer of the adsorbate, a is the effective thickness of the free adsorption layer in contact with vapor (Fig. 1b), which attains saturation at the maximum thickness of about five monolayers.

Powers (1965), using the BET isotherm, estimated in 1965 that a monomolecular water adsorption layer in cement paste was complete at $h = 12\%$ and a bimolecular one at 51%. This would imply that $c_T \approx 54$, which is the value used in the plot of BET isotherm in Fig. 1b. However, because of the new phenomena discussed here and in Part II which follows (Bazant and Bažant), this estimate of c_T is likely to be far too high.

Eq. (1) can be easily inverted

$$h = h(a) = A + \sqrt{A^2 + B} \tag{2}$$

where

$$A = \frac{Bc_T}{2}\left(1 - \frac{s_0}{a}\right), \quad B = \frac{1}{c_T - 1} \tag{3}$$

Hindered adsorption: Consider now a pore with planar rigid adsorbent walls parallel to the coordinates x and z, and a width $2y$ that is smaller than the combined width $2a$ of the free adsorption layers at the opposite walls given by Eq. (1). Then, the adsorbate has no surface in contact with the vapor and full free adsorption layers are prevented from building up at the opposite pore walls, i.e., the adsorption is hindered and a transverse pressure, p_d, called the disjoining pressure (Derjaguin, 1940), must develop. For water in C–S–H, which is highly hydrophillic, the adsorption layers can be up to 5

molecules thick, and so hindered adsorption can exist only in pores less than 10 molecules wide ($2y < 2.6$ nm). Here in Part I we deal solely with pores of such width. The hindered adsorption with disjoining pressure will develop when h is high enough to fill the pore. The hindered adsorbate communicates by diffusion along the pore with the vapor in an adjacent macropore.

In a process in which thermodynamic equilibrium is maintained, the chemical potentials μ of the vapor and its adsorbate, representing the Gibbs' free energy per unit mass, must remain equal. So, under isothermal conditions

$$\mathrm{d}\mu = \rho_a^{-1}(\mathrm{d}\tilde{p}_d + 2\mathrm{d}p_a)/3 = \rho_v^{-1}\,\mathrm{d}p_v \tag{4}$$

here ρ is the mass density of the vapor and ρ_a is the average mass density of the adsorbate (which probably is, in the case of water, somewhere between the mass density ρ_w of liquid water and ice). The superscript ˜ is attached to distinguish the disjoining pressure obtained by continuum analysis from that obtained later by discrete molecular considerations ($\tilde{p}_d = 0$ if the nanopore is not filled because the transverse pressure due to water vapor is negligible); $p_a = \pi_a/y$ is the in-plane pressure in the adsorption layer averaged through the thickness of the hindered adsorption layer; it has the dimension of N/m², and (in contrast to stress) is taken positive for compression; π_a is the longitudinal spreading 'pressure' in the adsorption half-layer of thickness y (here the term 'pressure' is a historically rooted misnomer; its dimension is not pressure, N/m², but force per unit length, N/m); π_a is superposed on the solid surface tension ga_s, which is generally larger in magnitude, and so the total surface tension, $\gamma = \gamma_s - p_a$, is actually tensile (see Bažant, 1972a, Fig. 2) (thus the decrease in spreading pressure with decreasing h causes an increase in surface tension, which is one of the causes of shrinkage).

Further note that if p_d and p_a were equal, the left-hand side would be $\mathrm{d}\mu = \rho_a^{-1}\,\mathrm{d}p_d$, which is the standard form for a bulk fluid. Also, in contrast to solid mechanics, the left-hand side of Eq. (4) cannot be written as $\epsilon_y\,\mathrm{d}p_d + 2\epsilon_x\,\mathrm{d}p_a$ because strains ϵ_x and ϵ_y cannot be defined (since the molecules in adsorption layers migrate and the difference between p_d and p_a is caused by the forces from solid adsorbent wall rather than by strains).

Consider now that the ideal gas equation $p_v\rho_v^{-1} = RT/M$ applies to the vapor (M=molecular weight of the adsorbate; e.g., for water $M = 18.02$ kg/kmole). Upon substitution into Eq. (4), we have the differential equation

$$\text{for } h \leq h_f: \quad \rho_a^{-1}\,\mathrm{d}p_a = (RT/M)\,\mathrm{d}p_v/p_v \tag{5}$$

$$\text{for } h > h_f: \quad \rho_a^{-1}(\mathrm{d}\tilde{p}_d + 2\,\mathrm{d}p_a)/3 = (RT/M)\,\mathrm{d}p_v/p_v \tag{6}$$

where h_f is the value of h at which the nanopore of width $2y$ gets filled, i.e., $h_f = h(y)$ based on Eq. (2). Factors 2 and 3 do not appear for $h < h_f$ because the free adsorbed layer can expand freely in the thickness direction. Integration of Eq. (4) under the assumption of constant ρ_a yields

$$\text{for } h \leq h_f: \quad p_a = \frac{\pi_a}{y} = \rho_a \frac{RT}{M}\,\ln h \tag{7}$$

$$\text{for } h > h_f: \quad \tilde{p}_d + 2(p_a - p_{af}) = 3\rho_a \frac{RT}{M}\,\ln \frac{h}{h_f} \tag{8}$$

where $p_{af} = p_a(h_f)$ is the longitudinal pressure when the nanopore just gets filled, i.e., when $a = y$.

It is now convenient to introduce the ratio of the increments of in-plane and disjoining pressures

$$\kappa = \mathrm{d}p_a/\mathrm{d}\tilde{p}_d \tag{9}$$

which we will call the disjoining ratio. If the adsorbate was a fluid, κ would equal 1. Since it is not, $\kappa \neq 1$. The role of κ is analogous to the Poisson ratio of elastic solids. A rigorous calculation of κ would require introducing (aside from surface forces) the constitutive equation relating p_a and p_d (this was done in Bažant and Moschovidis (1973), but led to a complex hypothetical model with too many unknown parameters).

We will consider κ as constant, partly for the sake of simplicity, partly because (as clarified later) κ is determined by inclined forces between the pairs of adsorbate molecules (Fig. 3b and c); κ should be constant in multi-molecular layers because the orientation distribution of these forces is probably independent of the nanopore width. Note that κ would be equal to 0 only if all these intermolecular forces were either in-plane or orthogonal (as in a rectangular grid, Fig. 3a).

For constant disjoining ratio κ, we may substitute $p_a = \kappa\tilde{p}_d$ in Eq. (8), and we get

$$\tilde{p}_d = \frac{\rho_a}{1 + 2\kappa} \frac{RT}{M}\,\ln \frac{h}{h_f} \tag{10}$$

For $\kappa = 0$, this equation coincides with Eq. (29) in Bažant (1972a) but, in view of Fig. 3, a zero κ must be an oversimplification.

According to this continuum model of hindered adsorption, which represents a minor extension of Bažant (1972a), the sorption isotherm of the adsorbate mass as a function of vapor pressure would have to be reversible. However, many classical and recent experiments (Powers and Brownyard, 1946; Feldman and Sereda, 1964; Rarick et al., 1995; Espinosa and Franke, 2006; Baroghel-Bouny, 2007) as well as recent molecular simulations (Bonnaud et al., 2010; Brochard et al., 2011, 2012) show it is not. Two mutually related mechanisms that must cause sorption irreversibility in nanopores with fixed rigid walls will be presented, one here in Part I, and one in Part II which follows (Bazant and Bažant).

3. Mechanism I: snap-through instability

The local transverse (or disjoining) pressure p_d can be determined from the transverse stiffness C_n, defined as $C_n = \Delta F / \Delta s$, where ΔF is the transverse resisting force per molecule and Δs is the change of spacing (or distance) between the adjacent monomolecular layers in a nanopore containing n monomolecular layers of the adsorbate. Since large changes of molecular separation are considered, C_n varies with s and should be interpreted as the secant modulus in the force–displacement diagram (Fig. 2b). For this reason, and also because many bond forces are inclined ('lateral interactions' (Nikitas, 1996; Cerofolini and Meda, 1998a, 1998b)) rather than orthogonal with respect to the adsorption layer (shown by the bars in Fig. 3), C_n is generally the same as neither the second derivative $d^2\Phi/dr^2$ of interatomic potential nor the first derivative dF/ds of force F (Fig. 2a and b).

To estimate C_n, one could consider various idealized arrangements of the adsorbate molecules (as depicted two-dimensionally for two different pore widths $2y$ in Fig. 3) and thus obtain analytical expressions for C_n based on the classical mechanics of statically indeterminate elastic trusses. However, in view of all the approximations and idealizations, it makes no sense to delve into these details.

Diverging nanopore: Consider now a wedge-shaped nanopore between two diverging planar walls of the adsorbent (Fig. 4a), having the width of $2y$, where $y = kx$. Here x is the longitudinal coordinate (Fig. 4), k is the constant (wedge inclination) and s_0 is the effective spacing of adsorbate molecules at no stress. In the third dimension, the width is considered to be also s_0. The adsorbate molecules are mobile and at the wide end (or mouth) of the pore they communicate with an atmosphere of relative vapor pressure h in the macropores.
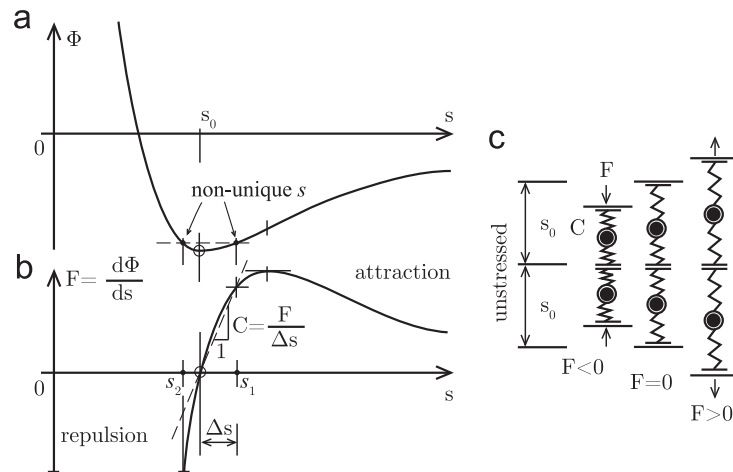

Fig. 2. (a) Interatomic pair potential; (b) the corresponding interatomic force and secant stiffness; and (c) interatomic forces between opposite pore walls visualized by springs.
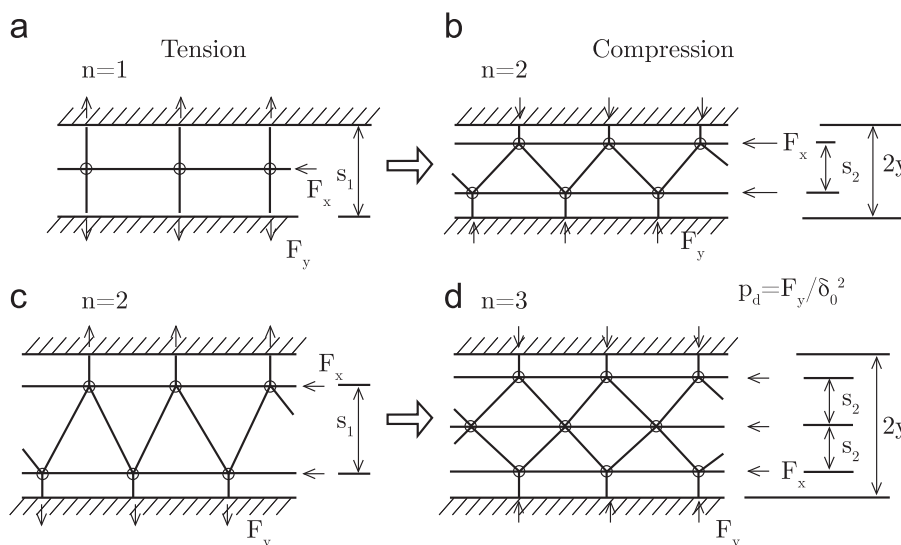

Fig. 3. Various simple idealized molecular arrangements between the walls of a nanopore.
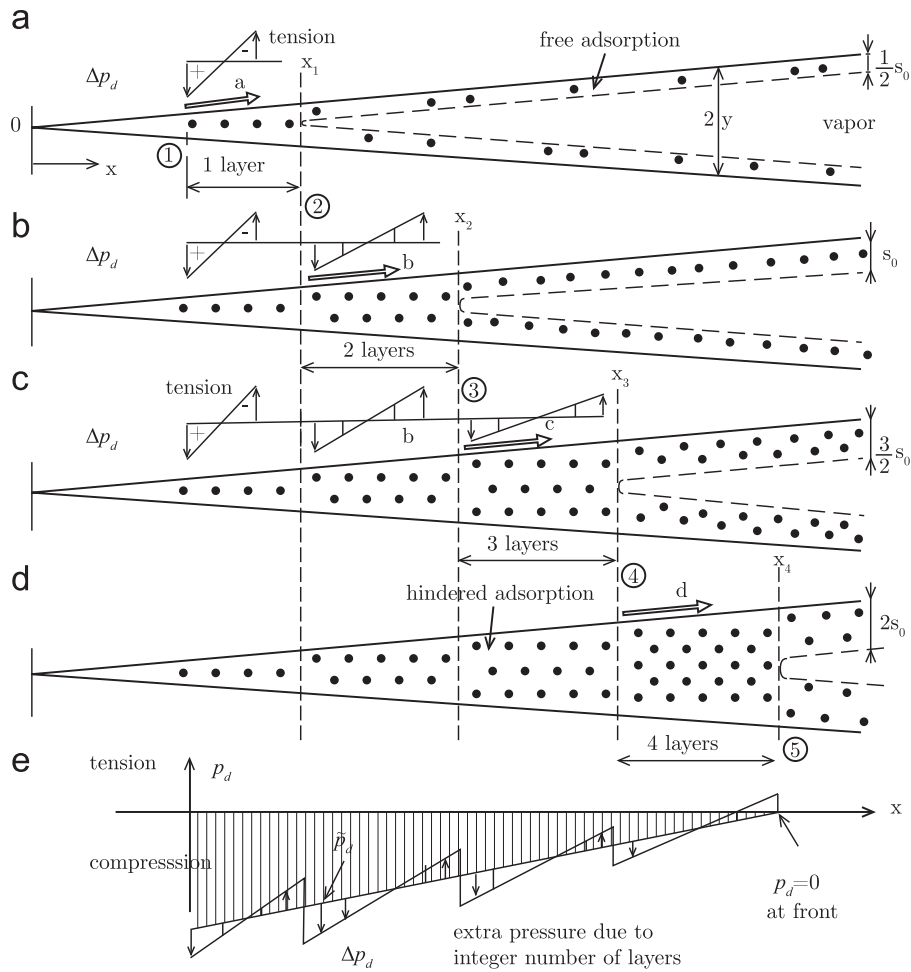
Fig. 4. Filling of a continuously diverging nanopore and disjoining pressures.

We assume the hindered adsorbed layer to be in thermodynamic equilibrium with the vapor in an adjacent macropore. This requires equality of the chemical potentials $\overline{\mu}$ *per molecule* ($\overline{\mu} = \mu/M$, the overbar being used to label a quantity per molecule). At the front of the portion of the nanopore filled by adsorbate, henceforth called the 'filling front' (marked by circled 2, 3 or 4 in Fig. 4), Eq. (10) of continuum thermodynamics gives a zero transverse pressure, $\tilde{p}_d = 0$, and so $\overline{\mu} = \overline{\mu}_a = \overline{\mu}_v$.

However, in the discrete treatment of individual molecules, the chemical potential can be altered by transverse tension or compression Δp_d (Fig. 4), which can develop at the filling front and act across the monomolecular layers unless the nanopore width $2y$ at the filling front happens to be an integer multiple of the unstrained molecular spacing s_0. We will call Δp_d the 'misfit' (part of) disjoining (or transverse) pressure, by analogy with the misfit strain energy for a dislocation core in the Peierls–Nabarro model (Hirth and Lothe, 1992).

The misfit pressure, which, at the filling front, represents the total transverse pressure (or stress), is determined by the average change Δs of spacing s between adjacent monomolecular layers, which is

$$\Delta s = 2kx/n - s_0 \quad (n = 1, 2, 3, \ldots) \tag{11}$$

where n is the number of monomolecular layers across the nanopore width and s_0 is the natural spacing between the adjacent monomolecular layers in free adsorption, i.e., when the transverse stress vanishes (note that for the triangular arrangements in Fig. 2b and c, s_0 is obviously less than the natural spacing of unstressed adsorbate molecules, shown as s_0 in Fig. 2a). So, the force between the molecules of the adjacent layers is $F = C\Delta s$ and the strain energy of the imagined springs connecting the molecules is $F\Delta s/2$ or $C(\Delta s)^2/2$ per molecule (if, for simplicity, a loading along the secant is considered).

The hindered adsorbed layer is in a multiaxial stress state, for which the total strain energy is the sum of the strain energies of the strain components. Since continuum thermodynamics gives zero disjoining (transverse) pressure p_d at the filling front, it suffices to add to $C_n(\Delta s)^2/2$ the chemical potential $\overline{\mu}_a$ per molecule at the filling front due to longitudinal pressure p_a only. So, in view of Eq. (10), the chemical potential per molecule at the filling front x_n^f with n monomolecular

Z.P. Bažant, M.Z. Bazant / J. Mech. Phys. Solids 60 (2012) 1644–1659

1651

layers is

$$\overline{\mu}_{f,n} = \frac{C_n}{2}\left(\frac{2kx_f}{n}-s_0\right)^2+\overline{\mu}_a \tag{12}$$

where again the overbar is a label for the quantities per molecule. Since $\tilde{p}_d = 0$ at the filling front x^*, the only source of $\overline{\mu}_n$ is the longitudinal spreading pressure p_a in the adsorption layer.

Let us now check whether at some filling front coordinate x^* (Fig. 4) the diverging nanopore is able to contain either n or $n+1$ monomolecular layers with the same chemical potential per molecule. For $n+1$ layers

$$\overline{\mu}_{f,n+1} = \frac{C_n}{2}\left(\frac{2kx}{n+1}-s_0\right)^2+\overline{\mu}_a \tag{13}$$

Setting $\overline{\mu}_n = \overline{\mu}_{n+1}$, we may solve for x. This yields the critical coordinate and critical pore width for which the molecules in n and $n+1$ monomolecular layers have the same chemical potential per molecule:

$$x_{f,n}^* = \frac{\sqrt{C_n}+\sqrt{C_{n+1}}}{\frac{1}{n}\sqrt{C_n}+\frac{1}{n+1}\sqrt{C_{n+1}}}\frac{s_0}{2k}, \quad y_{f,n}^* = 2kx_{f,n}^* \tag{14}$$

So, the critical relative pore width $2y_f^*/s_0$ at the filling front is a weighted harmonic mean of n and $n+1$ (and a simple harmonic mean if $C_n = C_{n+1}$).

Equality of the chemical potentials per molecule at the filling front for n and $n+1$ monomolecular layers in the same nanopore, which occurs for the pore width given by Eq. (14), implies that no energy needs to be supplied and none to be withdrawn when the number of monomolecular layers is changed between n and $n+1$. So, the equilibrium content of hindered adsorbate in the nanopore for a given chemical potential of vapor is non-unique. Similar to non-uniqueness of capillary surfaces, this non-uniqueness underlies the sorption–desorption hysteresis in the nanopores.

The possibility of non-uniqueness is evident from Fig. 2. For the same value of potential Φ, there are two states with different molecular separations s_1 and s_2, one corresponding to attraction (tension) and one to repulsion (compression), as seen on the horizontal line intersecting the curve of Φ in Fig. 2. Note that the secant stiffness for compression must be larger than it is for tension, which is a point neglected, for the sake of simplicity, in the foregoing calculation.

Misfit disjoining pressure: In view of Eq. (12), its value corresponding to $\overline{\mu}_n$ for n monomolecular layers in the nanopore is

$$p_{d,n} = C_n\left(s_0-\frac{2kx^*}{n}\right)+\tilde{p}_d(x_n) \tag{15}$$

where $\tilde{p}_d(x_n)$, based on continuum thermodynamics, is non-zero if $x_n \neq x_{f,n}$. In contrast to stress, the pressure is considered as positive when compressive. Replacing n with $n+1$, we find that the disjoining pressure makes a jump when the number of monomolecular layers in the nanopore changes from n to $n+1$

$$\Delta p_{d,n} = p_{d,n+1}-p_{d,n} = 2kx_n\left(\frac{C_n}{n}-\frac{C_{n+1}}{n+1}\right)+s_0(C_{n+1}-C_n) \tag{16}$$

(see Fig. 4). At the filling front, the jump is from transverse tension to compression (Fig. 5c).

Eq. (16) shows that the sudden jumps $\Delta p_{d,n}$ of the misfit pressures from tension to compression diminish with increasing n ($n=1,2,3,\dots$), as the nanopore is getting wider; see Figs. 4d and 5c. Therefore, the wider the pore is, the less effective the mechanism of snap-through instabilities is. It ceases to operate for pores of width $n > 10$, which are wider than the combined maximum thicknesses of two opposite adsorption layers (about 3 nm).

Note that, since the changes Δs of molecular distance are large, the C values depend on F or Δp_d (Fig. 2b). So, Eq. (16) is actually a nonlinear equation for Δp_d and its numerical solution would require iterations. But here we are aiming at conceptual explanation rather than numerical results.

Misfit chemical potentials and their effect on sorption isotherm: The variation of chemical potential at the filling front x_f is shown in Fig. 5d. Since transverse tension at the filling front gives the same chemical potential as transverse compression of equal magnitude, the misfit chemical potential, defined as the part of chemical potential due to p_d at the filling front, varies continuously, provided the pore width varies continuously, too; see Fig. 5d. This is because transverse tension gives the same chemical potential as transverse compression of equal magnitude.

The total chemical potential at the filling front is obtained by adding the chemical potential $\overline{\mu}_a(x_f)$ obtained from continuum thermodynamics, which yields the potential variation in Fig. 5e. Considering the relation of filling front coordinate x_f to the adsorbate mass w shown (in a smoothed form) in Fig. 5b, and the relation $h = e^{(M/RT)\mu_f}$, one can deduce the solid curve in Fig. 5e representing the diagram of equilibrium states of mass content w versus relative vapor pressure h in the macropore.

Why are the segments of the pressure variation in Fig. 5c linear, and why are the segments of the chemical potential variation in Fig. 5d–f parabolic? The reason is that the variation of nanopore width has been idealized as linear (and that the plots are made for constant C). These segments take different shapes for other width variations.

Sequential snap-throughs of adsorbate content: In sorption testing and most practical problems, the relative vapor pressure h is the variable that is controlled, and the adsorbate mass w is the response. Consequently, the states at the
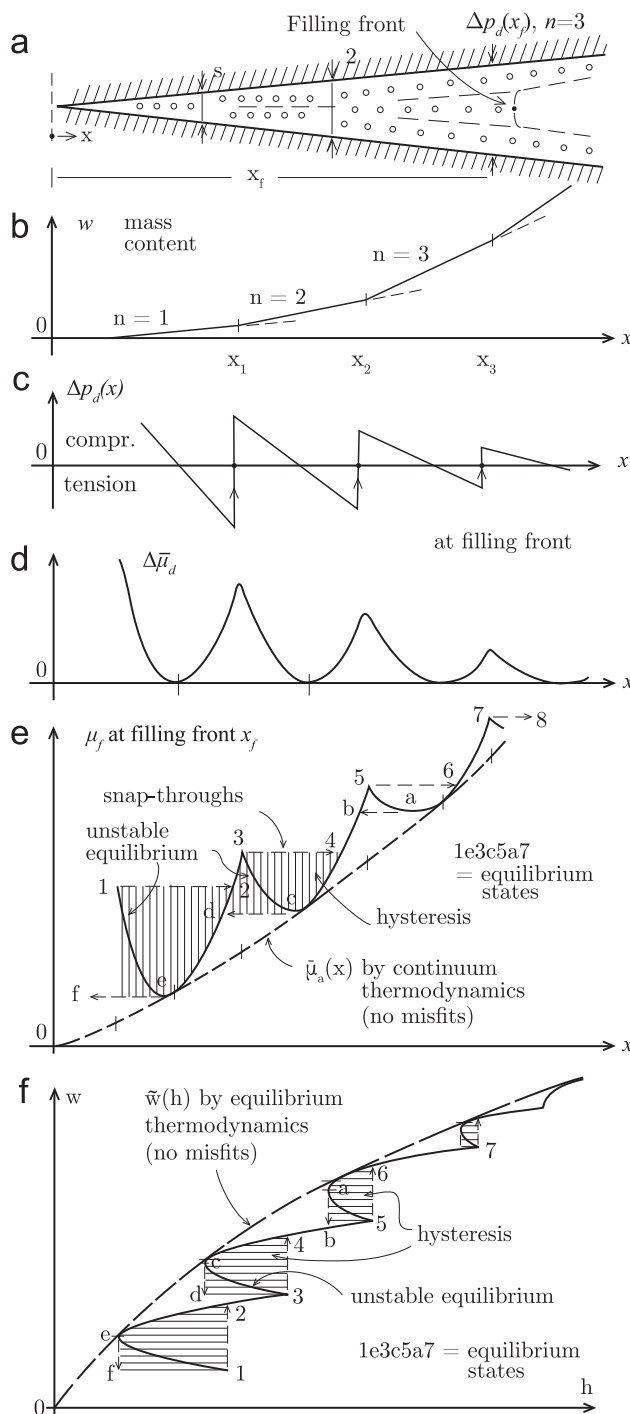
Fig. 5. Misfit disjoining pressures and chemical potentials in a continuously diverging nanopore, with dynamic snap-throughs of adsorbate content.

reversal points 1, 3, 5, 7 of the equilibrium diagram in Fig. 5 for the diverging nanopore are unstable. Likewise, the states at points 1, 3, 5, 7 in Fig. 6d for the nanopore of step-wise variable width. The loss of stability can be evidenced by checking that the molecular potential loses positive definiteness. Fundamental though such checks may be, it is simpler and more intuitive to argue in terms of infinitely small deviations dh from the equilibrium state.

Consider, e.g., that, in Fig. 5f or 6d, a sufficiently slow gradual increase of h has moved the equilibrium state from point 2 to point 3, which is a local maximum of h as a function of w. For a further infinitesimal increase dh, there is on the equilibrium diagram no longer any point close to point 3. So, borrowing a term from structural mechanics (Bažant and Cedolin, 1991), we realize that the adsorbate mass content w must dynamically 'snap through' at constant h along vertical line 34 to point 4. After dissipating the energy released along segment 34 (the rate of which depends on the lingering times of adsorbed molecules and diffusion along the hindered adsorbed layer; Bažant and Moschovidis, 1973), thermodynamic
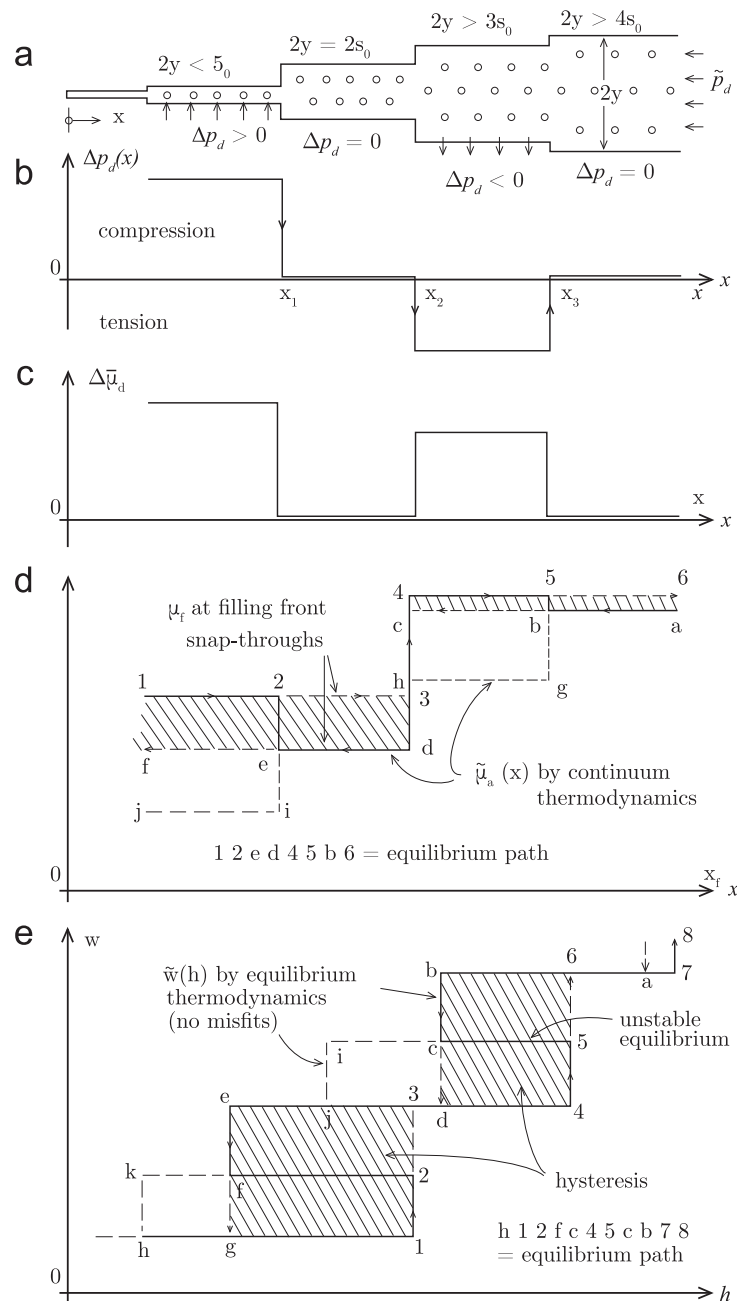
Fig. 6. Step-wise diverging nanopore and misfit disjoining pressures.

equilibrium is recovered at point 4. It is stable because a further infinitesimal increment of dh finds, next to point 4, an equilibrium state with adsorbate content incremented by dw.

If h is increased slowly enough further, the equilibrium system will move from point 4 to point 5 at which a local maximum of h is reached again and the loss of stability gets repeated, since a further increase dh can find equilibrium only after a dynamic snap-through to point 6. Each snap-through will release some energy which must be damped and dissipated by the system. So, the local maxima of h at points 1, 3, 5 and 7 are the critical states giving rise to the so-called 'snap-through instability' (Bažant and Cedolin, 1991). The equilibrium states on curved segments 1e2, 3c4 and 5a6 are unstable and can never be reached in reality.

The salient feature is that a different path $w(h)$ is followed when h is decreased. To show it, consider point 7 in Fig. 5f or 6d as the starting point. During a slow enough decrease h, the system will follow the stable states along segment 76a until a local minimum of h is reached at point a, which is the stability limit. Indeed, if h is further decremented by dh, there is no equilibrium state near point a. So, the equilibrium state a is unstable and the system will 'snap through' dynamically at constant h along path ab. At point b stable equilibrium is regained after sufficient time. When h is decreased further slowly enough, the equilibrium states move through segment b4c until again a local minimum of h is reached and stability is lost at point c. Thereafter, the system 'snaps through' along line cd to point d, where equilibrium is regained, etc.

In the diverging pore in Fig. 5, the snap-through means that when the equilibrium filling front reaches the critical points, x_1, x_2, or x_3, it will advance forward a certain distance at constant h, as fast as diffusion along the micropore, controlled by the lingering times of the adsorbate molecules, will permit.

The cross-hatched areas in between the sorption and desorption isotherms, such as area 34cd3 in Fig. 5e or 6d, represent sorption hysteresis. They also characterize energy dissipation.

Sequential snap-throughs for step-wise nanopore width variation: The diagrams in Fig. 5d–f are valid only for a micropore with continuously diverging rigid planar walls (Fig. 5a). This is, of course, an idealization. Because of the atomistic structure of pore walls, the pore width in reality varies discontinuously, as exemplified in Fig. 6a. The chance of a width exactly equal to an integer multiple of s_0 is small.

Consider that the jumps of nanopore width (Fig. 6a) occur at $x_1, x_2, x_3, \ldots$, and that at x_1 is narrower than s_0, at x_2 exactly equal to $2s_0$, and at x_3 wider than $3s_0$. Thus, the filling front in pore segment (x_1, x_2) is in transverse compression, in segment (x_2, x_3) at zero transverse pressure, and in segment (x_3, x_4) in transverse tension; see Fig. 6b. The corresponding strain energies, representing the misfit chemical potential $\Delta\overline{\mu}_d$ per molecule, have a pulse-like variation as shown in Fig. 6c. Continuum thermodynamics, which ignores the misfits, gives a monotonically rising staircase variation of the chemical potential $\tilde{\mu}_a(x)$ (per unit mass) as a function of the filling front coordinate x_f, represented by path *jiedhgba* (Fig. 6d). Superposing on this staircase the misfit chemical potential $\Delta\overline{\mu}_d$ (converted to unit mass), one gets the non-monotonic step-wise path of equilibrium states, shown by the bold line 12ed455b6 in Fig. 6d.

Taking into account the dependence of the adsorbate mass w in the nanopore on the filling front coordinate x_f, one can covert the diagram in Fig. 6d into the sorption isotherm in Fig. 6e, usually plotted as w versus h. The monotonic staircase *hkfejicba* would represent the equilibrium path if the misfit disjoining pressures were ignored.

When the rise of h, and thus μ_f, is controlled, the segments 23 and 56 in Fig. 6e are unstable and unreachable. Indeed, when h or μ_f is infinitesimally increased above point 2, there is no nearby equilibrium state, and so the system will 'snap through' dynamically to point 3. At that point, equilibrium is regained, and h and μ_f can be raised again, slowly enough to maintain equilibrium, along path 345. A similar dynamic snap-through is repeated along segment 56, after which the stable segment 678 can be followed. Likewise, in the diagram of μ_f versus the filling front coordinate x_f (Fig. 6d), forward snap-throughs at increasing μ_f (which is a monotonically increasing function of h) occur along segments 23 and 56.

When h or μ_f is decreased slowly enough from point 8, the stable equilibrium path 876bc is followed until stability is lost at point c (Fig. 6e). Then, the system snaps through dynamically from c to d, follows equilibrium path *def*, and snaps dynamically from f to g. Likewise, in Fig. 6d, backward snap-throughs at decreasing μ_f occur along segments bc and ef.

Obviously, the states on segments c5 and f2 in Fig. 6e, or 2e and 5e in Fig. 6d, can never be reached. They represent unstable equilibrium. The shaded areas g13eg and d46bd represent hysteresis, which leads to energy dissipation.

Snap-throughs in a system of nanopores: The diverging nanopore (Figs. 4, 5a and 6a) is not the only pore geometry producing sorption hysteresis. There are infinitely many such geometries. In the simple model of discrete monolayers pursued in Part I, the only geometry avoiding hysteresis due to sequential snap-throughs is hypothetical—the widths of all the nanopores would have to be exactly equal to the integer multiples of the natural spacing s_0 of monomolecular layers in free adsorption, so as to annul the misfit pressures. Below, we will show that if molecular coalescence is allowed in the lateral direction, then even these special pore geometries will exhibit sorption hysteresis, and so the effect is extremely general.

An essential feature of nanoporosity is that there are nanopores of many different thicknesses $2y$ densely distributed as shown in Fig. 7. At a given vapor pressure, all the nanopores that are narrower than a certain width $2y$ are filled by adsorbed water and the wider ones are empty, containing only vapor; see Fig. 7a, c and e.

As the relative pore pressure h is increased, larger and larger pores fill up. A critical state (or a local maximum of h) is reached for a pore width at which the misfit chemical potential $\Delta\mu_d$ due to misfit disjoining pressure is for n monomolecular layers equal to or larger than the misfit chemical potential for $n+1$ layers. After that state, the system loses stability and regains it only when all the nanopores up to a certain larger width get filled without increasing h. For decreasing h, the stability loss would occur for a different pore width.

The distribution of nanopore thicknesses $2y$ may be characterized by a continuous cumulative frequency distribution function $\varphi(y)$ that represents the combined volume of all the nanopores with thicknesses $< 2y$. This case, though, is not qualitatively different from the diverging nanopore studied previously. For $\varphi(y) \propto ky^2$, the nanopore system in Fig. 7 becomes mathematically equivalent to the linearly diverging nanopore studied before.

The way the hysteresis in the individual nanopores gets superposed to produce a pronounced hysteresis on the macroscale is schematically illustrated in Fig. 8.

Rough or non-matching nanopore surfaces: For hydrated cement, a smooth pore surface is surely an idealization, needed to render the calculations simple. In reality, the pore surface is irregular, random and rough. Recently, it has been shown (Yang et al., 2011) by MD simulations of nitrogen in carbon slit-pores that random surface roughness of approximately the same amplitude as the fluid molecule diameter effectively damps the oscillations of the disjoining pressure, compared to molecularly smooth surfaces. However, it is doubtful that this is true locally, for the disjoining intermolecular forces individually. The preceding observations regarding a system of nanopores applies to arbitrarily short nanopores, and a rough pore can be imagined as a series of very short smooth nanopores. The roughness aspect calls for deeper study.

Even if the nanopore surface is a regular atomic lattice, the spacing of surface atoms generally does not match the equilibrium spacing of adsorbate molecules along the pore. This imposes a wavy potential of transverse intermolecular forces with non-matching wavelength. This potential will alter the locations of the snap-throughs.
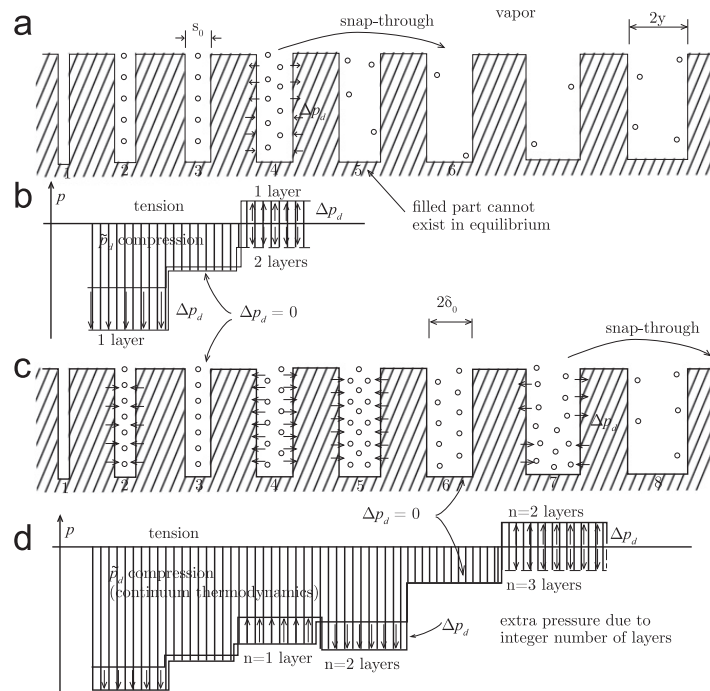
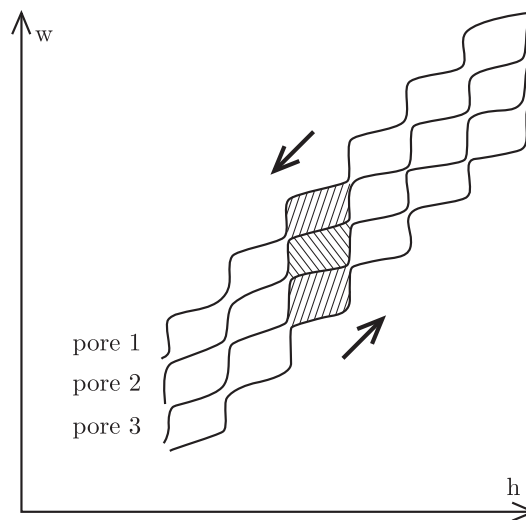**Fig. 7.** System of nanopores of different widths communicating through vapor phase.

Fig. 8. Superposition of hysteretic loops from different nanopores.

Temperature: The present analysis of snap throughs focuses on isolated, fixed molecular energy barriers and thus neglects some important thermal effects in the adsorbate. Temperature appears in the present analysis via the entropy of the vapor phase (which defines the humidity) and the reversible, continuum isotherm for multi-layer adsorption. The free energy barriers for snap through instabilities are related to discrete molecular inclined forces without accounting for entropic contributions and molecular rearrangements that constantly vary the barrier energy and structure. At low temperatures, this solid-like picture of the adsorbate with long-lived molecular states is valid, and snap throughs can occur by rare, thermally activated transitions over the energy barriers related to inclined molecular forces in non-uniform pore geometries.

This model, however, neglects the balance between the same attractive lateral interactions and the entropy of discrete molecular rearrangements on the surface, which can lead to 'phase separation' into low-density and high-density phases in the adsorbate (Gelb et al., 1999). Such effects dominate at low temperature (below the 'critical hysteresis temperature') and can lead to sorption hysteresis even in perfectly straight nanopores. Variations in the nanopore geometry, however, do provide additional free energy barriers for molecular condensation and snap throughs between different pore regions. As shown in Part II, these temperature-dependent phenomena can be treated using non-equilibrium statistical thermodynamics, which provides a general theory of molecular condensation in nanoporous solids building on this work.
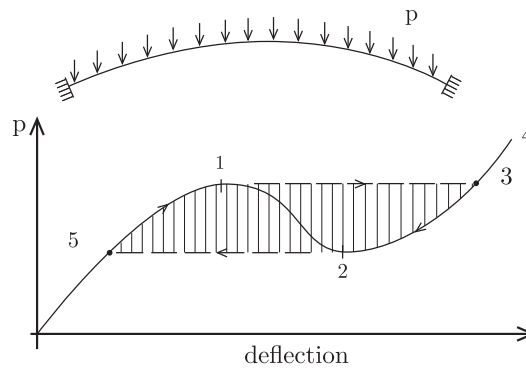
Fig. 9. Analogy with snap-through of an arch.

Analogy with snap-through buckling of flat arch: There is an instructive analogy with the snap-through buckling of elastic arches or shells under controlled load (Bažant and Cedolin, 1991, Fig. 9, p. 231). If the arch is flat enough and flexible enough not to fracture, the equilibrium diagram of total load p versus midspan deflection u follows the diagram sketched in Fig. 9. The segments 051 and 432 consist of stable states at which the potential energy is positive definite (i.e., has a strict local minimum). But this is not true for the equilibrium states on the segment 12, at which the potential energy does not have a strict local minimum.

Consider that load p is increased from point 0 up to the local maximum at critical point 1 (Fig. 9). If load p is increased further by an infinitesimal amount ddp, there is no nearby equilibrium state. The arch must follow at constant load the dynamic snap-through path 14, during which there is accelerated motion. The load difference from the equilibrium curve below represents the inertial force, which provides rightward acceleration. The arch gains kinetic energy up to point 3, swings over (along a horizontal line), and then vibrates at constant load about point 3 until the kinetic energy is dissipated by damping (without damping, it would vibrate indefinitely). Then, if the load is increased further, the arch moves through stable equilibrium states on the segment 34.

When the load is decreased, starting at point 4, the arch will follow the stable equilibrium states along segment 432 until a local minimum is reached at point 2. If the load is decreased further by an infinitesimal amount dP, there is no equilibrium state near point 2. So, the arch must snap through dynamically to point 5, the load being again balanced by inertia forces which provide leftward acceleration. During this snap-through the arch gains kinetic energy, swings over to the left of point 5 and vibrates about point 5 until the kinetic energy is dissipated by damping. Then, the load can be decreased further following the stable equilibrium states below point 5.

Note that even though the arch is elastic and the structure–load system is conservative, hysteresis is inevitable. During the cycle, the arch dissipates an energy equal to the cross-hatched area 51325 in Fig. 4.

Energy dissipated by hysteresis and material damage: The Gibbs free energy dissipated per unit mass of the nanoporous material is $dG = w\,d\mu$, where $d\mu = RT/M\,d\ln h$, which has in thermodynamic equilibrium the value for the adsorbate species in the vapor and for the adsorbed phases. Therefore, the free energy dissipated per unit volume of material due to the hysteresis during a complete cycle, e.g., a drying–wetting cycle of hardened cement paste, is

$$\Delta G = \frac{RT}{M} \oint \frac{w(h)}{h}\,dh \tag{17}$$

Since h is in the denominator, integrability, i.e., the finiteness of ΔG, requires that $\lim_{h\to 0} w/h = 1/h^n$, where $0 \le n < 1$. Graphically, ΔG is proportional to the area between the sorption and desorption isotherms in the diagram of w/h versus h (Fig. 10).

The energy could be dissipated in two ways:

(1) By internal friction in the adsorbed fluid during the dynamic snap-throughs (or the molecular coalescence phenomena discussed in Part II Bazant and Bažant) or
(2) by fracturing or plastic damage to the nanopore surfaces.

However, the latter seems unlikely since it could be associated with every disjoining pressure change and not particularly with the snap-through. The existence of the former is undeniable, and the point here is to show that the hysteresis is perfectly explicable without postulating any damage to the nanopore surface.

Anyway, the degree of material damage due to a drying–wetting cycle, if any, could be checked by measuring the strength or the fracture energy, or both, of the material before and after the cycle. This would have to be done slowly enough on thin enough specimens having drying half-times less than 1 h (< 1 mm thick for cement paste), in which the relative humidity h in the capillary pores can be changed without creating a significant gradient of h across the specimen wall (in thicker samples, most of the material damage is done by non-uniform shrinkage stresses engendered by non-uniformity of h across the wall thickness Bažant and Raftshol, 1982). Shrinkage and creep experiments on such specimens
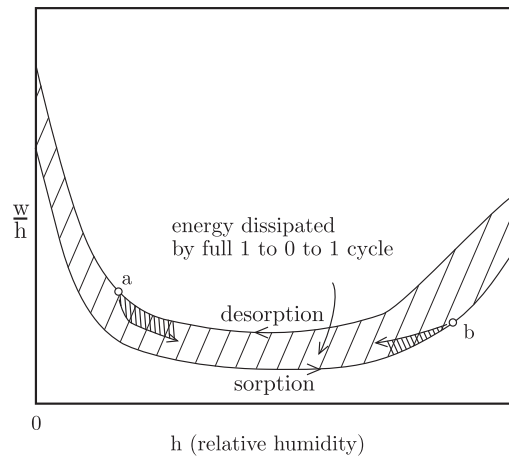
Fig. 10. Energy dissipated by sorption hysteresis on a full *h*-cycle 1→0→1 (shaded area), and dissipation during mid-range reversals (a, b).

have been performed at Northwestern (Bažant et al., 1976), but no cycles were performed and strength changes were not checked. It could also be checked whether the snap-throughs might be associated with the acceleration of concrete creep due to simultaneous drying, called the drying creep (or the Pickett effect).

Sorption potential: Note that, based on the derivation of Eq. (17), it further follows that

$$\beta = \frac{RT}{M}\frac{w}{h} = \frac{\partial G}{\partial h} \tag{18}$$

In other words, Gibbs's free energy per unit mass of adsorbate as a function of *h* is a potential for the adsorbate content parameter *β* during a one-way change of *h*.

Is the atomic crystal structure of pore walls relevant? The spacing of atoms in the pore walls imposes on the attractive potential a waviness whose wavelength generally differs from the in-plane spacing of the adsorbate molecules. However, it would be incorrect to consider the adsorbate molecule to jump over the peaks of this wavy attractive potential. The reason is that such jumps are not rare hopping processes. Unlike solids, the adsorbate molecules undergo constant vigorous rearrangements (except during solidification at extremely low temperature). Thus, they feel only the average surface properties and have strong entropic/steric interactions with the surface. In liquids and gases, the entropy prevails over bond enthalpy and prevents long-lived solid-like states connected by thermal hopping.

4. Conclusions of Part I

We can summarize the findings of the first part as follows:

1. One mechanism that must be causing sorption hysteresis at low vapor pressure is a series of snap-through instabilities causing path-dependent non-uniqueness of adsorbate content and dynamic jumps of water content of nanopores at constant vapor pressure.
2. The snap-through instabilities are a consequence of the discreteness of the adsorbate, which leads to non-uniqueness of mass content and to misfit disjoining (transverse) pressures due to a difference between the pore width and an integer multiple of the thickness of a transversely unstressed monomolecular layer of the adsorbate.
3. The hysteresis is explained by the fact that the snap-through instabilities for sorption and desorption follow different paths.
4. The wider the pore, the weaker the mechanism of snap-through instabilities. This mechanism cannot operate in pores wider than about 3 nm.
5. The snap-through instabilities are analogous to snap-through buckling of arches and shells, long known in structural mechanics. They cause hysteresis and energy dissipation even when the arch or shell is perfectly elastic and the load conservative.

If a quantitative version of this theory were developed, it might be possible to infer from the hysteresis the surface area and the size distribution of the nanopores filled by hindered adsorbate. Our preliminary analysis of snap-through instabilities suggests that the key to making this connection is to also account for inclined forces and 'lateral interactions', in the statistical thermodynamics of hindered adsorption. Part II will show that attractive lateral interactions generally lead to sorption hysteresis in any pore geometry due to molecular coalescence of the adsorbate (Bazant and Bažant).

Acknowledgment

References

Adolphs, J., Setzer, M.J., 1996. A model to describe adsorption isotherms. J. Colloid Interface Sci. 180, 70–76.

Adolphs, J., Setzer, M.J., Heine, P., 2002. Changes in pore structure and mercury contact angle of hardened cement paste depending on relative humidity. Mater. Struct. 35, 477–486.

Balbuena, P.B., Berry, D., Gubbins, K.E., 1993. Solvation pressures for simple fluids in micropores. J. Phys. Chem. 97, 937–943.

Baroghel-Bouny, V., 2007. Water vapour sorption experiments on hardened cementitious materials. Part I: essential tool for analysis of hygral behaviour and its relation to pore structure. Cem. Concr. Res. 37, 414–437.

Bažant, Z.P., 1970a. Constitutive equation for concrete creep and shrinkage based on thermodynamics of multi-phase systems. Mater. Struct. 3, 3–36. (reprinted in Wittmann, F.H. (Ed.), Fifty Years of Evolution of Science and Technology of Building Materials and Structures, RILEM, Aedificatio Publishers, Freiburg, Germany, 1997, pp. 377–410).

Bažant, Z.P., 1970b. Delayed thermal dilatations of cement paste and concrete due to mass transport. Nucl. Eng. Des. 24, 308–318.

Bažant, Z.P., 1972a. Thermodynamics of interacting continua with surfaces and creep analysis of concrete structures. Nucl. Eng. Des. 20, 477–505.

Bažant, Z.P., 1972b. Thermodynamics of hindered adsorption with application to cement paste and concrete. Cem. Concr. Res. 2, 1–16.

Bažant, Z.P., 1975. Theory of creep and shrinkage in concrete structures: a précis of recent developments. In: Nemat-Nasser, S. (Ed.), Mechanics Today (Am. Acad. Mech.), vol. 2. Pergamon Press, pp. 1–93.

Bažant, Z.P., Asghari, A.A., Schmidt, J., 1976. Experimental study of creep of hardened cement paste at variable water content. Mater. Struct. (RILEM, Paris) 9, 190–279.

Bažant, Z.P., Cedolin, L., 1991. Stability of Structures: Elastic, Inelastic, Fracture and Damage Theories. Oxford University Press, New York (2nd ed. Dover Publications, 2003; 3rd ed. World Scientific Publishing, Singapore, NJ, London, 2010).

Bažant, Z.P., Kaplan, M.F., 1996. Concrete at High Temperatures: Material Properties and Mathematical Models. Longman (Addison-Wesley), London (2nd ed. Pearson Education, Edinburgh, 2002).

Bažant, Z.P., Moschovidis, Z., 1973. Surface diffusion theory for the drying creep effect in Portland cement paste and concrete. J. Am. Ceram. Soc. 56, 235–241.

Bažant, Z.P., Raftshol, W.J., 1982. Effect of cracking in drying and shrinkage specimens. Cem. Concr. Res. 12, 209–226. Disc. 797–798.

Bažant, Z.P., Thonguthai, W., 1978. Pore pressure and drying of concrete at high temperature. Proc. ASCE, J. Eng. Mech. Div. 104, 1058–1080.

Bazant, M.Z., Bažant, Z.P. Theory of sorption hysteresis in nanoporous solids: II. Molecular coalescence, J. Mech. Phys. Solids, http://dx.doi.org/10.1016/j.jmps.2012.04.015, this issue.

Bonnaud, P.A., Coasne, B., Pellenq, R.J.-M., 2010. Molecular simulation of water confined in nanoporous silica. J. Phys.: Condens. Matter, 284110. (15pp.).

Brochard, L., Vandamme, M., Pellenq, R.J.-M., Teddy, F.-C., 2011. Adsorption-induced deformation of microporous materials: coal swelling induced by CO_2?CH_4 competitive adsorption langmuir, 28 (5), 2659–2670. Publication Date (Web): December 20, 2011 (Article) http://dx.doi.org/10.1021/la204072d.

Brochard, L., Vandamme, M., Pellenq, R.J.-M., 2012. Poromechanics of microporous media. J. Mech. Phys. Solids 60 (4), 606–622. http://dx.doi.org/10.1016/j.jmps.2012.01.001.

Brunauer, S., 1943. The Adsorption of Gases and Vapors. Princeton University Press, Princeton, NJ, p. 398.

Brunauer, S., Emmett, P.T., Teller, E., 1938. Adsorption of gases in multi-molecular layers. J. Am. Chem. Soc. 60, 309–319.

Cerofolini, G.F., Meda, L., 1998a. A theory of multilayer adsorption on rough surfaces in terms of clustering and melting BET piles. Surf. Sci. 416, 402–432.

Cerofolini, G.F., Meda, L., 1998b. Clustering and melting in multilayer equilibrium adsorption. J. Colloid Interface Sci. 202, 104–123.

Coasne, B., Galarneau, A., Di Renzo, F., Pellenq, R.J.-M., 2008a. Molecular simulation of adsorption and intrusion in nanopores. Adsorption 14, 215–221.

Coasne, B., Di Renzo, F., Galarneau, A., Pellenq, R.J.-M., 2008b. Adsorption of simple fluid on silica surface and nanopore: effect of surface chemistry and pore shape. Langmuir 24, 7285–7293.

Coasne, B., Galarneau, A., Di Renzo, F., Pellenq, R.J.-M., 2009. Intrusion and retraction of fluids in nanopores: effect of morphological heterogeneity. J. Phys. Chem. C 113, 1953–1962.

Derjaguin, B.V., 1940. On the repulsive forces between charged colloid particles and the theory of slow coagulation and stability of lyophile sols. Trans. Faraday Soc. 36, 203. 730.

Espinosa, R.M., Franke, L., 2006. Influence of the age and drying process on pore structure and sorption isotherms of hardened cement paste. Cem. Concr. Res. 36, 1969–1984. (Figs. 2, 6, 16).

Feldman, R.F., Sereda, P.J., 1964. Sorption of water on compacts of bottle hydrated cement. I: the sorption and length-change isotherms. J. Appl. Chem. 14, 87.

Feldman, R.F., Sereda, P.J., 1968. A model for hydrated Portland cement paste as deduced from sorption-length change and mechanical properties. Mater. Struct. 1 (6), 509–520.

Gelb, L.D., Gubbins, K.E., Radhakrishnan, R., Sliwinska-Bartkowiak, M., 1999. Phase separation in confined systems. Rep. Prog. Phys. 62, 1573–1659.

Hall, C., Hoff, D., Taylor, S.C., Wilson, M.A., Yoon, B.G., Reinhardt, H.-W., Sossoro, M., Meredith, P., Donald, A.M., 1995. Water anomaly in capillary liquid absorption by cement-based materials. J. Mater. Sci. Lett. 14, 1178–1181.

Hirth, J.P., Lothe, J., 1992. Theory of Dislocations. Kreiger.

Jennings, H.M., 2000. A model for the microstructure of calcium silicate hydrate in cement paste. Cem. Concr. Res. 30, 101–116.

Jennings, H.M. Pores and viscoelastic properties of cement paste, submitted for publication.

Jennings, H.M., Bullard, J.W., Thomas, J.J., Andrade, J.E., Chen, J.J., Scherer, G.W., 2008. Characterization and modeling of pores and surfaces in cement paste: correlations to processing and properties. J. Adv. Concr. Technol. 6 (1), 5–29.

Jönson, B., Wennerström, H., Nonat, A., Cabane, B., 2004. Onset of cohesion in cement paste. Langmuir 20, 6702–6709.

Jönson, B., Nonat, A., Labbez, C., Cabane, B., Wennerström, H., 2005. Controlling the cohesion of cement paste. Langmuir 21, 9211–9221.

Malani, A., Ayappa, K.G., Murad, S., 2009. Influence of hydrophillic surface specificity on the structural properties of confined water. J. Phys. Chem. 113, 13825–13839.

Nikitas, P., 1996. A simple statistical mechanical approach for studying multilayer adsorption: extensions of the BET adsorption isotherm. J. Phys. Chem. 100, 15247–15254.

Pellenq, R.J.-M., Kushima, A., Shashavari, R., Van Vliet, K.J., Buehler, M.J., Yip, S., Ulm, F.-J., 2010. A realistic molecular model of cement hydrates. Proc. Nat. Acad. Sci. 106 (38), 16102–17107.

Powers, T.C., 1965. Mechanism of shrinkage and reversible creep of hardened cement paste. In: International Conference on the Structure of Concrete, Imperial College, London, Paper G1. Cement & Concrete Association, UK.

Powers, T.C., 1966. Some observations on the interpretation of creep data. Bull. RILEM (Paris), 381.

Powers, T.C., Brownyard, T.L., 1946. Studies of the physical properties of hardened portland cement paste. Part 2. Studies of water fixation. J. Am. Concr. Inst. 18 (3), 249–336.

Rarick, R.L., Bhatty, J.W., Jennings, H.M., 1995. Surface area measurement using gas sorption: application to cement paste. In: Skalny, J., Mindess, S. (Eds.), Material Science of Concrete IV, American Ceramic Society, pp. 1–41. (Chapter 1).

Scherer, G.W., 1999. Structure and properties of gels. Cem. Concr. Res. 29, 1149–1157.

Smith, D.E., Wang, Y., Chaturvedi, A., Whitley, H.D., 2006. Molecular simulations of the pressure, temperature, and chemical potential dependencies of clay swelling. J. Phys. Chem. B 110, 20046–20054.

Thomas, J.J., Allen, A.J., Jennings, H.M., 2008. Structural changes to the calcium hydrate gel phase of hydrated cement with age, drying and resaturation. J. Am. Ceram. Soc. 91 (10), 3362–3369.

Vandamme, M., Brochard, L., Lecampion, B., Coussy, O., 2010. Adsorption and strain: the CO_2-induced swelling of coal. J. Mech. Phys. Solids 58, 1489–1505.

Yang, K., Lin, Y., Lu, X., Neimark, A.V., 2011. Solvation forces between molecularly rough surfaces. J. Colloid Interface Sci. 362, 382–388.

Theory of sorption hysteresis in nanoporous solids: Part II Molecular condensation

Martin Z. Bazant [a],[*], Zdeněk P. Bažant [b]

[a] Chemical Engineering and Mathematics, Massachusetts Institute of Technology, Cambridge, MA 02139, United States
[b] Civil Engineering and Materials Science, Northwestern University, 2145 Sheridan Road, CEE/A135, Evanston, IL 60208, United States

ABSTRACT

Motivated by the puzzle of sorption hysteresis in Portland cement concrete or cement paste, we develop in Part II of this study a general theory of vapor sorption and desorption from nanoporous solids, which attributes hysteresis to hindered molecular condensation with attractive lateral interactions. The classical mean-field theory of van der Waals is applied to predict the dependence of hysteresis on temperature and pore size, using the regular solution model and gradient energy of Cahn and Hilliard. A simple "hierarchical wetting" model for thin nanopores is developed to describe the case of strong wetting by the first monolayer, followed by condensation of nanodroplets and nanobubbles in the bulk. The model predicts a larger hysteresis critical temperature and enhanced hysteresis for molecular condensation across nanopores at high vapor pressure than within monolayers at low vapor pressure. For heterogeneous pores, the theory predicts sorption/desorption sequences similar to those seen in molecular dynamics simulations, where the interfacial energy (or gradient penalty) at nanopore junctions acts as a free energy barrier for snap-through instabilities. The model helps to quantitatively understand recent experimental data for concrete or cement paste wetting and drying cycles and suggests new experiments at different temperatures and humidity sweep rates.

© 2012 Elsevier Ltd. All rights reserved.

1. Introduction

As introduced in Part I (Bažant and Bazant, this issue), a long-standing puzzle in the thermodynamics of concrete or cement paste and other nanoporous solids is the pronounced hysteresis of the sorption/desorption isotherm at low vapor pressure (Powers and Brownyard, 1946; Feldman and Sereda, 1964, 1968; Rarick et al., 1995; Scherer, 1999; Jennings et al., 2008; Adolphs et al., 2002; Espinosa and Franke, 2006). Typical experimental data for wetting/drying cycles in concrete is shown in Fig. 1, and similar behavior can be observed (or expected) in many other important situations, such as water sorption in dry soils or wood, carbon sequestration in porous absorbents, and natural gas recovery from nanoporous shales. At low vapor pressures, well below the saturation pressure, very little bulk liquid exists in the larger pores, and so the observed hysteresis cannot be attributed to the classical "ink-bottle effect" of capillarity from continuum fluid mechanics (Cohan, 1938; Brunauer, 1943). Moreover, in nanopores, the Laplace tension of a continuous meniscus can

* Corresponding author. Tel.: +1 617 258 7039; fax: +1 617-258-5766.
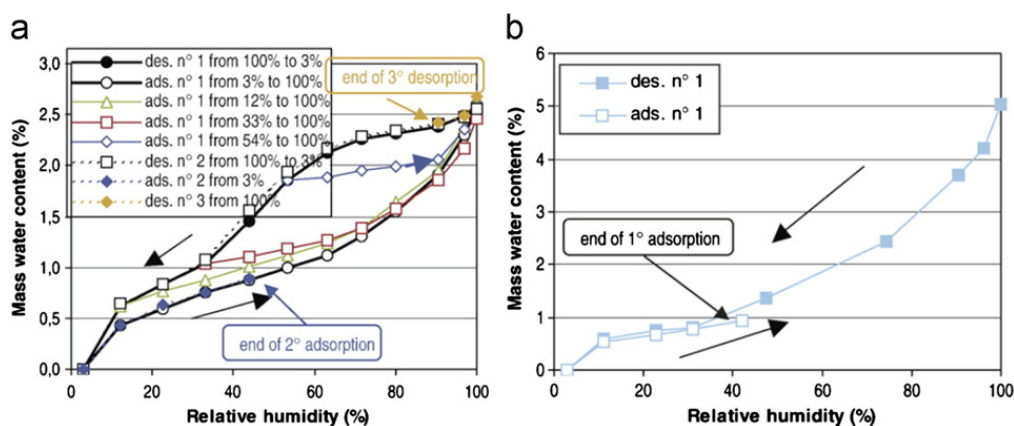 *E-mail address:* bazant@mit.edu (M.Z. Bazant).

Fig. 1. Experimental data for isothermal water–vapor desorption and sorption cycles in concrete at different temperatures. (a) Pronounced hysteresis at $T=23\,°C$. (b) Suppressed hysteresis at $T=44\,°C$. [Reproduced from Fig. 2(e) and (g) of Baroghel-Bouny (2007) with permission.]

easily exceed the tensile strength of the liquid. So it is widely believed that adsorbate layers must be uniformly spread over the entire internal surface area at low vapor pressure and unable to coalesce into nonuniform patches or droplets.

This thinking underlies the ubiquitous method of determining the internal surface area of porous media by fitting the sorption isotherm to the Brunauer–Emmett–Teller (BET) equation of state (Brunauer et al., 1838), which is strictly valid only for a statistically homogeneous adsorbate on a flat surface. Since the BET isotherm is perfectly reversible, the internal surface area can only be unambiguously inferred from one type of measurement, either sorption or desorption, starting from a well defined reproducible initial state. Typically, the BET fit is made for sorption starting from very low vapor pressure, assuming that the internal surface is initially bare, but it is troubling to neglect the desorption data, which would imply a different BET internal surface area, without a theory to explain its origin. Moreover, if a mathematical theory could be developed, then in principle one could extract more complete information about the internal pore structure, such as the statistical distributions of pore thickness or pore area, from the history dependence of sorption and desorption.

If one insists on the validity of any reversible adsorption isotherm (not only BET), then the only way to explain the observed hysteresis is to invoke changes in the accessible internal surface area, e.g. due to chemical transformations or structural damage (Feldman and Sereda, 1968; Thomas et al., 2008; Rarick et al., 1995; Espinosa and Franke, 2006). As a result, this picture of "pore collapse" and subsequent reopening upon desorption and sorption, respectively, is firmly entrenched, but it is noteworthy that, sixty years after the first observations of sorption hysteresis in concrete and cement paste, no mathematical theory has emerged to justify this assumption or make any testable theoretical predictions. For example, it is not clear how the pore collapse hypothesis could explain the strong dependence of sorption hysteresis in concrete on temperature and chemical composition of the vapor observed in recent experiments (Baroghel-Bouny, 2007), as shown in Fig. 1, or how it could be reconciled with the measured shrinkage values. While some adsorption-related structural changes surely occur in cement paste and concrete and other nanoporous solids, especially at high vapor pressures, the repeatability of sorption hysteresis (after the first few cycles) and the relatively small concomitant macroscopic deformations seem inconsistent with the very drastic changes to the pore structure at the nanoscale required by the pore-collapse hypothesis.

In this work, we show that, due to molecular discreteness, hysteresis is a natural and unavoidable feature of sorption in nanoporous solids with *fixed* pore geometries. In Part I (Bažant and Bazant, this issue), we showed that misfit pressures due to discrete molecular forces around heterogeneities in the nanopore geometry generally provide local energy barriers for the passage of the adsorbate-vapor interface, consistent with evidence from molecular dynamics simulations (Pellenq and Levitz, 2002; Coasne et al., 2007, 2008a, 2008b, 2009). As the thermodynamic driving force is increased by changing the vapor pressure, the interface remains pinned at the heterogeneity until a sudden "snap-through instability" occurs, analogous to snap-through buckling of a flat arch. This theory is also reminiscent of the Peierls–Nabarro model of dislocation motion in crystals, where the misfit strain energy due to discrete molecular forces in the dislocation core provides the crucial resistance to dislocation motion, which cannot be predicted by continuum elasticity (Hirth and Lothe, 1992). A common feature of both theories is the assumption of a layered solid-like material undergoing sudden, localized rearrangements in response to a driving force that overcome the effective "lattice resistance". An important difference between nanopore sorption and dislocation motion, however, is that there is no reference crystal structure or long-range order in the adsorbate, and so much more dramatic molecular rearrangements, such as wetting phase transformations, are possible. Predicting such phase transformations and their dependence on temperature requires a more detailed molecular model.

Here, in Part II, we consider sorption from the general perspective of statistical thermodynamics and develop a simple mathematical theory that connects hysteresis to inter-molecular forces. The model is quantitatively consistent with the concrete sorption data in Fig. 1 and suggests new directions for experiments and simulations to further develop the theory. The key insight is that sorption hysteresis is possible at sufficiently low temperature in any fixed surface geometry, as long

as the adsorbed molecules have a short-range attraction. Although weaker than the orthogonal forces that bind the adsorbate to the surface, such attractive lateral forces within the adsorbate itself promote condensation into stable high density patches below a critical temperature, regardless of the pore geometry. This phenomenon can be inhibited by geometrical or chemical heterogeneities on the surface, but molecular condensation can also occur in homogeneous pores or on flat surfaces, as the metastable homogeneous adsorbate phase separates into stable low-density and high-density phases within the porous structure.

Before we begin, let us explain our choice of terminology. The term "capillary condensation" has been used to describe wetting/de-wetting transitions on surfaces, which comprise a well-studied class of phase separation phenomena in confined systems (Gelb et al., 1999). We avoid the use of this term because in many fields, such as cement and concrete research (which motivates our work), the term "capillary water" refers to liquid water at high vapor pressure in large ($> 1 \, \mu m$) pores, which can be modeled by continuum fluid mechanics with constant gas/liquid surface tension. Here, we suggest the term "molecular condensation" to refer to the phase separation of discrete adsorbed molecules in nanopores at low vapor pressure, which requires a statistical mechanical treatment.

2. Mean-field theory of molecular condensation

2.1. Capillarity at the molecular scale

The macroscopic continuum theory of capillarity cannot be applied to very thin adsorbate layers, whose individual molecules interact strongly with the surface – and each other (Israelachvili, 1992; Rowlinson and Widom, 1984; de Gennes, 1985; Gelb et al., 1999). The density of an adsorbate is generally heterogeneous and lies between that of the bulk liquid and vapor phases, due to attractive forces with the surface which stabilize individual adatoms and (upon contact with a second surface) give rise to disjoining pressure. These "orthogonal forces" allow adsorbed molecules to be distributed over a surface without maintaining close lateral contacts. In a nanoscale pore, the total energy of the missing lateral bonds would be grossly overestimated, if they were approximated by sharp, continuous surfaces using the bulk surface tension and the nanoscale curvature. Instead, one must develop a theory that takes "lateral forces" between discrete adsorbate molecules explicitly into account.

The theory of snap-through instabilities in nonuniform pore geometries from Part I is an example of such an approach, but the effect of attractive lateral forces is much more general and can lead to sorption hysteresis even in perfectly uniform geometries. The basic idea is already illustrated by the simplest case of monolayer adsorption on a flat bare surface or monolayer-thick pore, as shown in Fig. 2. (The latter problem is equivalent to lithium insertion and extraction in a crystalline nanoparticle in a Li-ion battery (Singh et al., 2008; Burch and Bazant, 2009; Bai et al., 2011), and we apply similar concepts and models for adsorption dynamics Bazant, 2011.) As humidity increases during sorption (left), the dilute homogeneous adsorbate *a* becomes thermodynamically unstable and separates *b* into locally stable low-density and high-density phases, which quickly grow and merge into a stable homogeneous adsorbate at high density *c*. As humidity then decreases during desorption (right), the homogeneous phase *d* destabilizes and coalesces to form the stable, dense phase *e*, which quickly shrinks and leaves behind a stable, homogeneous low-density adsorbate *f*. The sketches in Fig. 2 assume nucleation of the second phase at the pore openings, although other phase-separation pathways are possible.

The key point is that molecular condensation, or separation into low-density and high-density adsorbate phases, is history dependent and occurs by triggering the sudden instability of a metastable state. The specific pore geometry is largely irrelevant. Spontaneous phase separation of the adsorbate is mathematically analogous to the snap-through instability of shells and arches, but the physical interpretation in terms of buckling failure may not always apply. More importantly, in order to predict the effect of temperature on sorption hysteresis, one must go beyond mechanical analogs and consider the statistical thermodynamics of adsorption.
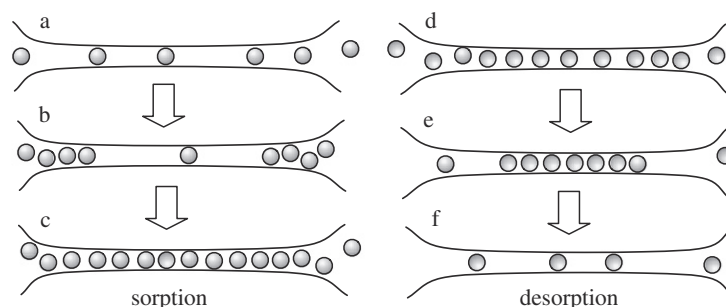

Fig. 2. Molecular condensation in a straight, monolayer-thick pore during sorption (left) and desorption (right) from the vapor at low temperature. Attractive lateral forces lead to the spontaneous separation of high-density and low-density adsorbate phases from metastable homogeneous phases. Analogous thermodynamic instabilities of the adsorbate distribution would also occur in thicker pores or flat surfaces, only across a different range of relative humidities, depending on the free energies of adsorption and lateral interaction. In non-uniform pores, the snap-through instability is another manifestation of this general phenomenon, driven by attractive lateral (or inclined) forces in the adsorbate. It naturally leads to sorption hysteresis without invoking any changes in pore structure.

2.2. Thermodynamics of adsorption with lateral forces

Consider a nanopore or surface film, whose state is described by a dimensionless filling $\Theta = \Gamma_w/\Gamma_1$, which may depend on lateral position x. The Gibbs free energy per surface site g can be expressed for a homogeneous adsorbate as follows:

$$g_{hom}(\Theta,x) = g_{mix}(\Theta,x) - \Delta g_a(x)\Theta \tag{1}$$

where g_{mix} is the free energy of mixing in the pore volume $V_s(x)$ associated with surface site x, which contains an expected number $\Theta(x)$ of adsorbate molecules, whose free energy change (per molecule) due to adsorption from the vapor phase is

$$\Delta g_a = k_B T \ln c_0 + \Delta q_a \tag{2}$$

The first term is a reference entropy, expressed in terms of a dimensionless concentration c_0 (as in BET theory) and Boltzman's constant k_B, and the second term, Δq_a, is the latent heat of adsorption minus that of liquefaction per site. To focus on molecular effects, here in Part II we define energies per particle, rather than per mole as in Part I ($\Delta Q_a/RT = \Delta q_a/k_B T$), and we drop the overbars for ease of notation. Lateral interactions among adsorbate molecules are included g_{mix}, e.g. according to the regular solution model of the next section. Orthogonal surface-adsorbate forces are treated separately via Δg_a. In the case of pairwise interactions, the enthalpic contribution can be expressed as

$$\Delta q_a = \int_{V_s} d\vec{r} \int_S d\vec{r}_s \Phi^s(|\vec{r} - \vec{r}_s|)p_s(\vec{r}\,|\,\vec{r}_s) \tag{3}$$

where the $\Phi^s(r)$ is the pair potential between adsorbate and surface molecules, $p_s(\vec{r}\,|\,\vec{r}_s)$ is the conditional probability density of finding a surface molecule at $\vec{r}_s$ anywhere in the solid volume S given an adsorbate molecule at $\vec{r}$ in the pore volume $V_s(x)$ associated with site x. In an isotropic bulk liquid, the pair correlation function $g(r)$ is defined by $p_s(\vec{r}\,|\,\vec{r}') = 4\pi r^2 g(r)$ where $r = |\vec{r} - \vec{r}'|$, but here the pore surface breaks symmetry.

Due to attractive lateral interactions, at sufficiently low temperature the homogeneous free energy of mixing $g_{mix}(\Theta)$ becomes non-convex and leads to at least two local minima in the total free energy, corresponding to stable high-density (liquid-like) and low-density (vapor-like) adsorbate phases on the surface, as shown in Fig. 3(a). A common tangent construction connecting the two local minima, which restores convexity across the "miscibility gap", provides the mean free energy of a phase separated system consisting of appropriate proportions of the immiscible endpoint phases (neglecting interphasial tension, discussed below). Phase separation is illustrated by sketches in Fig. 2, whose labels correspond to the letters in Fig. 3. During sorption, the homogeneous adsorbate passes the low-density free energy minimum a, destabilizes and drops down to the common tangent upon phase separation b, and becomes homogeneous again after passing the high-density free energy minimum c. A similar free-energy path is followed in reverse during desorption, only the free-energy overshoot in the metastable homogeneous adsorbate occurs at high density rather than low density. This is the fundamental source of hysteresis.

The connection with sorption hysteresis becomes more clear from the "diffusional" chemical potential of the homogeneous adsorbate:

$$\mu_{hom} = \frac{dg_{hom}}{d\Theta} = \frac{dg_{mix}}{d\Theta} - \Delta g_a \tag{4}$$

which is the net free energy change to add a molecule (and remove any vacant site). As sketched in Fig. 3(b), a non-convex free energy corresponds to a non-monotonic chemical potential versus composition. In equilibrium, the chemical potential of an adatom equals that of a vapor molecule:
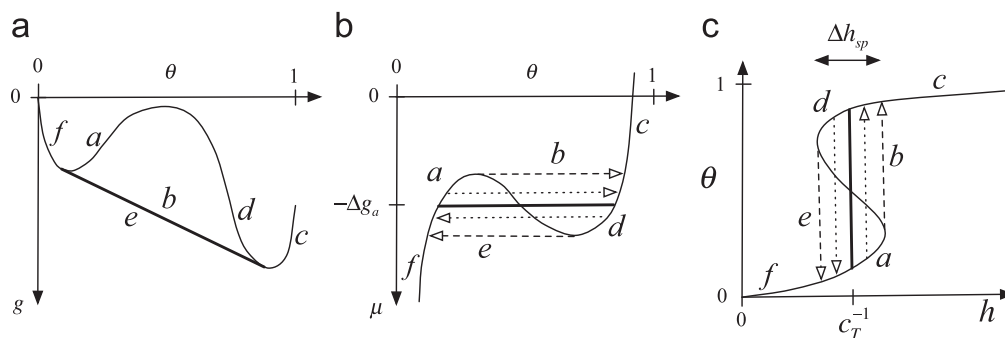
$$\mu_v = k_B T \ln h \tag{5}$$

Fig. 3. Effects of lateral forces on adsorption. (a) Gibbs free energy per site g versus dimensionless filling Θ of adsorbate. The homogeneous free energy g_{hom} (thin solid line) is made convex by a common tangent construction (thick solid line), which corresponds to phase separation into high and low density regions (neglecting interphasial tension). (b) Chemical potential μ per site for homogeneous (thin solid) and phase separated (thick solid) states. (c) The corresponding filling fraction versus relative humidity h for quasi-equilibrium between the adsorbate and vapor. Hysteresis during adsorption ($a \rightarrow b \rightarrow c$ in Fig. 10) or desorption ($d \rightarrow e \rightarrow f$) results from the delay in phase separation due to either nucleation (dotted lines) or spinodal decomposition (dashed lines).

where we set the zero of chemical potential in the saturated vapor phase ($h=1$). Setting $\mu_{hom} = \mu_v$ yields the equilibrium sorption curve (Θ vs h) for homogeneous filling of the nanopore, shown in Fig. 3(c). The non-convex free energy is seen to correspond to a non-invertible sorption curve with three degenerate filling fractions over the "spinodal range" of humidities, Δh_{sp}. Over the corresponding spinodal gap of filling fractions, where the free energy loses convexity ($d^2 g_{hom}/d\Theta^2 < 0$) and the chemical potential decreases with concentration ($d\mu_{hom}/d\Theta < 0$), the homogeneous adsorbate is linearly unstable with respect to the growth of infinitesimal perturbations of the concentration profile (spinodal decomposition). This leads to sorption hysteresis with varying humidity, as represented by the dashed lines in Fig. 3.

It is possible for phase separation to occur for any metastable composition within the miscibility gap, but outside the spinodal gap, a sufficiently large critical nucleus of the second phase is required. In the typical case of heterogeneous nucleation, phase separation is triggered at nanopore defects or boundaries, as sketched in Fig. 2. If nucleation occurs before spinodal decomposition, then phase separation occurs with less overshoot of the chemical potential plateau and smaller sorption hysteresis, as denoted by the dotted lines in Fig. 3 (b) and (c), respectively. For sufficiently slow humidity variations, the nanopore should be able to reversibly follow the convex equilibrium free energy surface without any hysteresis, but depending on experimental conditions, the required nucleation and growth may not have enough time to occur. In the absence of nucleation, the spinodal humidity range Δh_{sp} provides a convenient upper bound on the equilibrium sorption hysteresis, and so we now proceed to calculate it using a simple model.

2.3. Regular solution model

The simplest mean-field model of adsorption with lateral forces is the regular solution model for a binary mixture (Guggenheim, 1952; Cahn and Hilliard, 1958; Baluffi et al., 2005), whose free energy of mixing,

$$g_{mix} = k_B T[\Theta \ln \Theta + (1-\Theta)\ln(1-\Theta)] + \omega\Theta(1-\Theta) \tag{6}$$

comes from the continuum limit of a lattice gas of filled and empty sites. The first two terms represent the configurational entropy of particles and holes in the lattice, and the last term represents the enthalpy of mixing, expressed as a particle-hole interaction. The lattice gas could represent individual adsorbate molecules in a monolayer, either on a free surface or in a flat one-molecule-thick nanopore as in Fig. 2. As discussed below, the same model could also provide a first approximation of hindered multilayer adsorption, where the particles and holes represent coarsened molecular droplets and bubbles spanning the interior of a nanopore. Therefore, we will proceed to analyze sorption hysteresis in general terms without yet referring a specific pore geometry.

Lateral adsorbate-adsorbate forces are captured by the regular solution parameter, ω, equal to the mean energy of pairwise attraction between adsorbed molecules,

$$\omega = \int_{V_s} d\vec{r} \int_P d\vec{r}\,' \frac{1}{2} \Phi(|\vec{r} - \vec{r}\,'|) p(\vec{r}\,|\,\vec{r}\,') \tag{7}$$

where $\Phi(r)$ is the pair potential between adsorbate molecules, $p(\vec{r}\,|\,\vec{r}\,')$ is the conditional probability density of finding a molecule at $\vec{r}\,'$ anywhere in the pore volume P given a molecule at $\vec{r}$ in the site volume V_s. (The factor $\frac{1}{2}$ avoids double counting pair interactions.) Note that Δg_a and ω depend on position in a heterogeneous pore, whose geometry or surface chemistry varies with position.

As shown in Fig. 4(a), the homogeneous free energy of mixing reflects a competition between entropy, which favors mixing ($\Theta = \frac{1}{2}$) and enthalpy, which favors de-mixing or phase separation ($\Theta = 0, 1$). At high temperature, entropy dominates, and the free energy is convex with a minimum at $\Theta = \frac{1}{2}$. Below a critical temperature,

$$T_c = \frac{\omega}{2k_B} \tag{8}$$

enthalpy (due to attractive lateral forces) begins to dominate entropy, and there is a pitchfork bifurcation (in the mathematical sense), leading to two local minima of the free energy density, corresponding to stable high-density and low-density phases. The miscibility gap is the range of metastable homogeneous compositions, bounded by the circles in Fig. 4(a). The homogeneous chemical potential is given by

$$\mu_{hom} = k_B T \ln \frac{\Theta}{1-\Theta} + \omega(1-2\Theta) - \Delta g_a \tag{9}$$

which is plotted for different temperatures in Fig. 4(b) to illustrate the onset of non-monotonic behavior for $T < T_c$. The spinodal gap is the range of unstable compositions, bounded by circles in Fig. 4(b).

The corresponding adsorption isotherm, obtained by setting $\mu_{hom} = \mu_v$, is given by

$$c_T h = \left(\frac{\Theta_{hom}}{1-\Theta_{hom}}\right) \exp\left(\frac{\omega(1-2\Theta_{hom})}{k_B T}\right) \quad \text{where } c_T = c_0 \exp\left(\frac{\Delta q_a}{k_B T}\right) \tag{10}$$

and plotted in Fig. 4(c). At high temperature, we recover the classical Langmuir isotherm without lateral interactions,

$$\Theta_{hom} \sim \frac{c_T h}{1 + c_T h} \quad \text{for } T \gg T_c \tag{11}$$
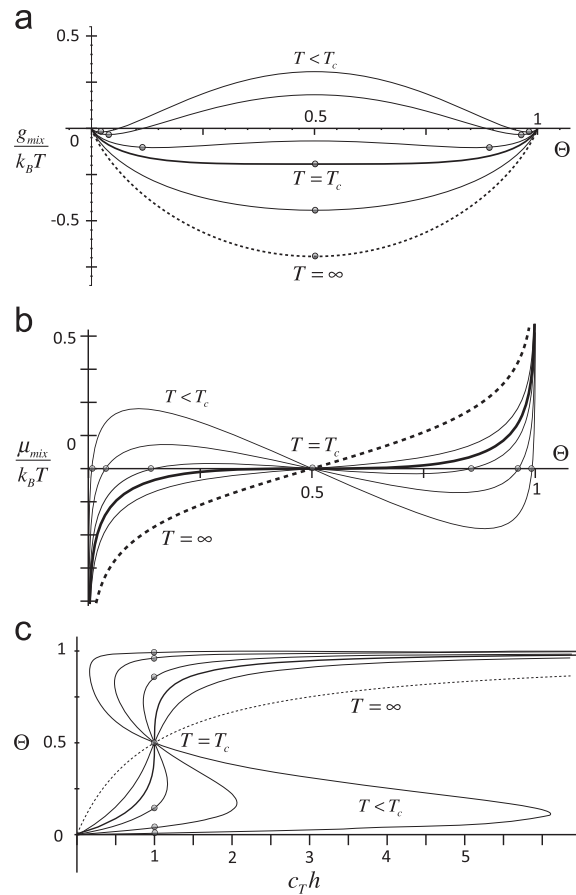
Fig. 4. Thermodynamics of condensation in the regular solution model for an adsorbed monolayer with attractive intermolecular forces ($\omega > 0$). (a) Free energy of mixing versus filling fraction. (b) Homogeneous chemical potential (shifted by the adsorption energy) versus filling fraction. (c) Filling fraction versus humidity. Below the critical temperature $T_c = \omega/2k_B$, enthalpy dominates entropy; the free energy is non-convex; the chemical potential is non-monotonic; and the adsorption isotherms are multi-valued, leading to hysteresis. Curves are shown for $T/T_c = \frac{2}{5}, \frac{4}{7}, \frac{4}{5}, 1$ (heavy solid), $\frac{4}{3}$, and ∞ (dashed). Gray circles on all curves correspond to local free energy minima (stable or metastable states).

Below the critical point, $T < T_c$, the modified Langmuir isotherm with lateral interactions becomes non-monotonic, and the sorption curve exhibits hysteresis.

The spinodal humidity range, which provides an upper bound on the humidity hysteresis in this model, can be derived analytically:

$$\Delta h_{sp} = \frac{2}{c_0} f\left(\frac{T_c}{T}\right) \exp\left(-\frac{\Delta q_a}{k_B T}\right) \tag{12}$$

where the Arrhenius temperature dependence is augmented by a prefactor

$$f(u) = \frac{c_T \Delta h_{sp}}{2} = (2u-1)\sinh\nu - \nu\cosh\nu \quad \text{where } \nu = 2\sqrt{u(u-1)}, \ u = \frac{T_c}{T} = \frac{\omega}{2k_B T} \tag{13}$$

An important prediction of this model is that *sorption hysteresis decreases with increasing temperature and vanishes as a power law at the critical point*:

$$\Delta h_{sp} \sim \frac{8}{3c_T}\left(\frac{T_c}{T} - 1\right)^{3/2} \quad \text{as } T \to T_c \tag{14}$$

The same $\frac{3}{2}$ critical exponent also arises in the temperature dependence of the interfacial tension between the low-density and high-density phases in the van der Waals (1893) theory of capillarity and the related Cahn and Hilliard (1958) model of phase separation, which we consider in the next section. (In structural mechanics, this scaling relation is analogous to Koiter's 2/3-power law for the difference between the critical load at symmetric bifurcation of a perfect structure and the stability limit of imperfect structures with vanishing imperfections (Bažant and Cedolin, 1991). There is also Koiter's 1/2-power law for the bifurcation of a perfect system that is asymmetric, and we would expect analogous scaling, $\Delta h_{sp} \propto (T_c - T)^2$ in a different model with broken symmetry in the entropy and/or enthalpy density around $\Theta = \frac{1}{2}$.) More generally, the theory of critical phenomena provides many ways for nontrivial power law scalings to arise, $\Delta h_{sp} \propto (T_c - T)^\nu$, and the exponent ν is best determined by experiment for a given material.
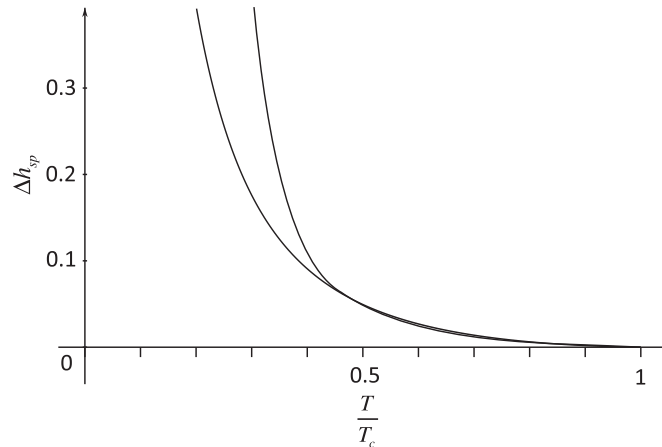
Fig. 5. Analytical prediction of the temperature dependence of sorption hysteresis, based on the regular solution model for lateral interactions in the adsorbate. The change in relative humidity across the spinodal range Δh_{sp} is plotted against reduced temperature T/T_c, where we set $c_T = 54$ for monolayer water adsorption in cement paste or concrete. We also neglect the weak temperature dependence of c_T, for the typical case where adsorption forces are much stronger than lateral forces ($\Delta q_a \geqslant 2k_B T_c = \omega$). The exact solution (12) and (13) (solid curve) is well approximated over this range by the asymptotic power law at the critical point (14) (dashed curve). At higher temperatures, $T > T_c$, molecular condensation is thermodynamically unfavorable due to the dominance of entropy over enthalpy.

As shown in Fig. 5, the critical power law (14) is a good approximation of the exact formula (12) and (13) over a broad temperature range corresponding to typical hysteresis values, $\Delta h < 10$. In these formulae, the weak dependence of c_T on temperature can be neglected if orthogonal adsorption forces are much stronger than lateral intermolecular forces, $\Delta q_a \geqslant 2k_B T_c = \omega$, which is always the case whenever there is significant adsorption from the vapor. (Otherwise, bulk liquid condensation would occur before surface adsorption.) For water adsorption in cement paste or concrete, this assumption is consistent with an early estimate of $\Delta q_a/k_B = \Delta Q_a/R = 2700$ K (Bažant and Najjar, 1972), which is likely to be much larger than T_c, as discussed below (see also Bažant and Kaplan, 1996, p. 210).

In such cases, the dominant temperature dependence in (12) comes from the prefactor (13), which vanishes at the critical point. Physically, sorption hysteresis disappears above the critical temperature because entropy, which promotes uniform surface coverage, then dominates the enthalpy of lateral interactions, which promotes molecular condensation. This is a very general effect, which will also arise in more complicated models (e.g. for multilayer adsorption Seri-Levy and Avnir, 1993; Nikitas, 1996; Cerofolini and Meda, 1998a, 1998b), as long as the lateral interactions among adsorbed molecules are attractive.

3. Molecular condensation on bounded surfaces

3.1. Interphasial tension

The foregoing theory describes sorption hysteresis for an infinite pore or surface, since it considers only the homogeneous free energy per site. In a finite system, phase separation is hindered by the interfacial (or "interphasial") tension between immiscible stable phases, below the critical temperature. The standard mathematical model of interphasial tension is based on the concept of a diffuse interface of continuously varying density, first introduced by van der Waals (1893) in his original "thermodynamic theory of capillarity" and still used today to describe surface wetting by thin liquid films (de Gennes, 1985; Cahn, 1977; Widom, 1999; Gouin and Gavrilyuk, 2008). The same model has also been used to describe disjoining pressure in liquid-filled nanopores (Gouin, 2009), albeit without making connections to adsorption isotherms and sorption hysteresis in nanoporous solids. Modern interest in this approach and many subsequent extensions sprang from the celebrated paper of (Cahn and Hilliard, 1958), which used the regular solution model to rederive and extend key results of (van der Waals, 1893) and paved the way for phase-field models in materials science (Thornton et al., 2003; Baluffi et al., 2005).

Given the homogeneous free energy (1) per discretized pore volume $V_s(\vec{r})$ (associated with fixed sites on the nearby pore surface), the total free energy G of an arbitrary (possible multiply connected) pore geometry can be expressed as an integral over the pore volume:

$$G[\Theta, S] = \int d\vec{r} \left[g_{hom}(\Theta, \vec{r}) + \frac{1}{2} \nabla\Theta \cdot \boldsymbol{K}(\vec{r}) \nabla\Theta \right] \tag{15}$$

which is a functional of $\Theta(\vec{r})$, the dimensionless filling fraction of the volume $V_s(\vec{r})$ (e.g. measured in monolayers, and possibly larger than one for a site volume spanning a nanopore) and $S(\vec{r})$, a function prescribing the surface geometry of the pore (e.g. via a level-set or phase-field description). The coefficient $\boldsymbol{K}$ in the second term is the "gradient penalty tensor", which approximates corrections to the free energy density due to density variations, as well as the interphasial tension (see below). In principle, both g_{hom} and $\boldsymbol{K}$ depend on position within the pore geometry specified by S. In Eq. (15), we neglect the mechanical energy stored in the solid phase (Thornton et al., 2003; Meethong et al., 2007b; Cogswell and

Bazant, 2011), in order to emphasize our prediction that hysteresis can occur in nanoporous solids whose mechanical deformation, if any, is too small to affect the equilibrium distribution of the adsorbate. It would be straightforward to incorporate mechanical response of the solid matrix in a more sophisticated model, e.g. Cogswell and Bazant (2011).

The diffusional chemical potential is given by the functional derivative with respect to composition:

$$\mu = \frac{\delta G}{\delta \Theta} = \mu_{hom} - \nabla \cdot \boldsymbol{K} \nabla \Theta \tag{16}$$

where $\mu_{hom} = g'_{hom}$ is the homogeneous chemical potential (4). Physically, this corresponds to the free energy change upon creating a continuum "molecule" represented by a delta function at $\overrightarrow{r}$. Outside the spinodal range, setting chemical potential $\mu = $ constant yields one uniform solution, corresponding to a stable homogeneous phase. Within the spinodal range, there are three uniform solutions, two stable and one unstable, and $\mu = $ constant yields a Beltrami differential equation, whose nontrivial solution corresponds to a phase separated system with a diffuse phase boundary. In the regime of strong phase separation $\omega \gg k_B T$ or $T \ll T_c$, the width λ of the phase boundary scales as

$$\lambda = \sqrt{\frac{K}{\omega}} \tag{17}$$

in each eigendirection of the $\boldsymbol{K}$ tensor, and the corresponding interphasial tension (energy/area) is

$$\gamma = \rho_s \sqrt{K\omega} \tag{18}$$

where ρ_s is the density of sites per volume, or the inverse of the single-site volume (Cahn and Hilliard, 1958; Burch and Bazant, 2009).

3.2. Suppressed condensation in small pores

The tendency for phase separation is reduced in small systems, as the phase interface area to bulk volume ratio increases. More precisely, both the spinodal range (Cahn, 1961) and miscibility gap (Nauman and Balsara, 1989; Nauman et al., 1991; Burch and Bazant, 2009) shrink and ultimately disappear, as the system size becomes comparable to the phase boundary thickness. For phase separation in solid materials, if the two phases have different equilibrium volumes, then elastic coherency strain energy further reduces the miscibility and spinodal gaps and can eliminate phase separation (Cogswell and Bazant, 2011).

The suppression of phase transformations with decreasing system size is a universal phenomenon, which is drawing attention in other fields and has important technological applications. For example, it controls the "ultimate fineness", or minimum feature size, of polymer-in-polymer microdispersions (Nauman and Balsara, 1989; Nauman et al., 1991). Recently, it has also played a major role in the development of high-rate Li-ion batteries using lithium iron phosphate (Li_xFePO_4), which has a strong tendency for phase separation into Li-rich and Li-poor domains. Ironically, when it was first explored as an insertion cathode material in microparticle form, Li_xFePO_4 was predicted to be good for "low power applications" as a result of slow phase separation dynamics and related mechanical deformations (Padhi et al., 1997), but today, in nanoparticle form, it is capable of ultrafast battery discharge (in tens of seconds) while maintaining long cycle life (Kang and Ceder, 2009). In addition to size-dependent diffusivity (Malik et al., 2010), the main reasons that "nano is different" may be the shrinking of the miscibility gap (Meethong et al., 2007a, 2007b; Burch and Bazant, 2009; Wagemaker et al., 2011; Cogswell and Bazant, 2011) and the dynamical suppression of phase separation (Malik et al., 2011; Bai et al., 2011; Cogswell and Bazant, 2011). Analogous phenomena must also occur for vapor sorption in nanopores, as we now explain.

Consider a homogeneous adsorbate $\Theta = \Theta_0$ in a straight pore or flat surface whose longest lateral dimension is L. For example, in the case of a perfect cylindrical pore, we set L equal to the maximum of its length and diameter. This state will be linearly stable to sinusoidal perturbations of wavevector $\overrightarrow{k}$, given by $\Theta(\overrightarrow{r}) = \Theta_0(1 + \epsilon e^{i\overrightarrow{k}\cdot\overrightarrow{r}})$, if the perturbation increases the chemical potential, which implies

$$\frac{\partial \mu_{hom}}{\partial \Theta}(\Theta_0) + \overrightarrow{k} \cdot \boldsymbol{K} \overrightarrow{k} > 0 \tag{19}$$

The second term is strictly positive, so in an infinite system, where arbitrarily long wavelength perturbations ($k \to 0$) with vanishing gradient energy are possible, the spinodal range is defined by setting the first term to zero, as above. In a finite system, however, there is a minimum wavelength for perturbations set by the boundary conditions, e.g. given by $k_{min} = \pi/L$ for constant concentration boundary conditions, reflecting adsorption equilibrium at the farthest ends of the pores. As a result, the spinodal range of unstable compositions, determined by $\mu < 0$, is generally reduced (Cahn, 1961; Nauman and Balsara, 1989; Burch and Bazant, 2009).

The corresponding spinodal humidity range $\Delta h_{sp}(L)$, defined as the jump in the homogeneous isotherm humidity between the spinodal points satisfying $\mu(\Theta,L) = 0$, is given by the same formula as derived above, Eqs. (12) and (13), but only with a length-dependent critical temperature:

$$T_c(L) = T_c^\infty \left(1 - \frac{\pi^2 \lambda^2}{2L^2}\right) \quad \text{where} \quad T_c^\infty = \frac{\omega}{2k_B} \tag{20}$$
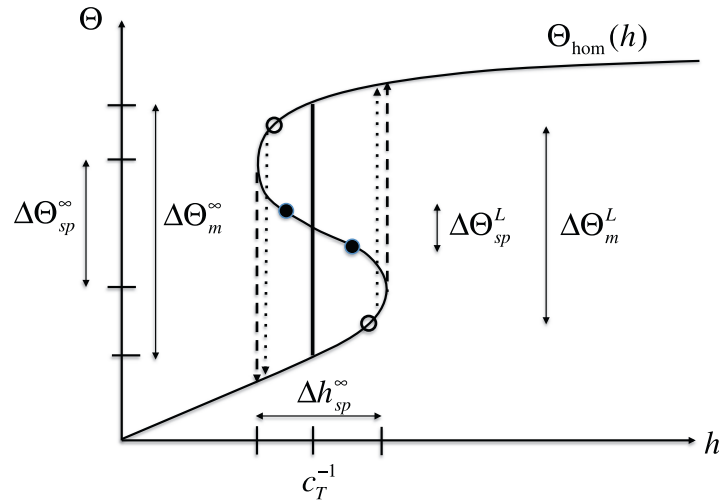
Fig. 6. Molecular condensation on a bounded surface of maximum dimension L (e.g. length or diameter of a cylindrical pore), where humidity h is controlled (rather than the mean filling fraction Θ). If nucleation is possible, then, as the miscibility gap $\Delta\Theta_m^L$ shrinks (open circles) and the nucleation rate decreases with decreasing pore size, the hysteresis (dotted lines) increases up to the maximum set by the spinodal humidity range, Δh_{sp}^∞. (b) In the absence of nucleation, the adsorbate undergoes sudden transitions at the infinite-system spinodals (dashed lines), prior to reaching the reduced spinodal gap $\Delta\Theta_{sp}^L$ (black points).

The critical point is depressed as the ratio of the system size to the phase boundary thickness λ/L decreases. For very small systems, $L < L_c = \pi\lambda/\sqrt{2}$, the critical temperature vanishes, and the homogeneous state is linearly stable, even at zero temperature. In simple physical terms, molecular condensation is only possible on surfaces whose length L is large enough to accommodate an equilibrium phase boundary of thickness λ.

3.3. Enhanced hysteresis in small pores

One might expect hysteresis to be suppressed in short pores, due to the reduced spinodal and miscibility gaps, but this is not the case since it is the humidity, not the filling fraction, that is experimentally controlled. The basic physics is sketched in Fig. 6. First consider the possibility of nucleation, where the second phase is created by fluctuations over the surface or at defects or pore edges. As the pore size is decreased, there are fewer sites for nucleation, and the reduced nucleation probability enhances hysteresis by preserving the homogeneous state as the humidity is varied. Even if nucleation is very fast, the reduced miscibility gap Δh_{hom}^L increases the corresponding humidity range of hysteresis, up to the limit set by Δh_{sp}^∞.

In the absence of nucleation, phase separation must occur by spinodal decomposition, which is also suppressed in short pores. If the humidity passes out of the spinodal range, then the adsorbate can pass into the infinite-system spinodal gap Δh_{hom}^∞ while remaining uniform. After the overshoot, it experiences a strong thermodynamic driving force to vary the concentration until the new homogeneous equilibrium state is reached, and phase separation may not have enough time to occur during this sudden transition. (This non-equilibrium transition state has recently been called a "quasi-solid solution" Bai et al., 2011.) As a result, the infinite-system spinodal humidity range, $\Delta h_{sp}^\infty(T)$, given by Eqs. (12)–(14), provides a robust estimate of sorption hysteresis in finite-length pores of any size if nucleation is too slow to occur over experimental time scales.

4. Molecular condensation in single nanopores

4.1. Theory of hindered multilayer adsorption

A general continuum model of adsorption in nanoporous media of arbitrary geometry could be based on the van der Waals (or Cahn–Hilliard) model, Eq. (15), where $\Theta(\vec{x})$ is the local mean density of the adsorbate at a point in the pore. The main difference with monolayer adsorption is that the adsorption free energy $\Delta g_a(\vec{x})$ would depend on $\vec{x}$ and reflects the decay of surface forces with distance from the pore walls, including screening effects due to the other molecules. The local interaction energy, $\omega(\vec{x})$, would also depend on position, approaching a bulk value as the influence of surface forces decays with distance from the nearest wall. The gradient penalty $K(\vec{x})$ would represent the local free energy difference associated with broken or frustrated molecular bonds (the nanoscale analog of gas-liquid surface tension), and this, too, would generally depend on position.

The dynamics of the concentration profile in such a model would be described by the Cahn–Hilliard equation (Baluffi et al., 2005; Naumann and He, 2001):

$$\frac{\partial\Theta}{\partial t} = \nabla \cdot [M\Theta\nabla\mu] \tag{21}$$

where the chemical potential $\mu(\Theta,\vec{x})$ is given by (16) and the diffusional particle mobility $M(\Theta,\vec{x})$ generally depends on the concentration and position. For example, in the foregoing regular solution model for the first monolayer, the mobility

should be proportional to the free volume, $M = M_0(1-\Theta)$ (this effect was omitted in early models and yields a "modified Cahn–Hilliard equation" Naumann and He, 2001). More generally, to account for finite pores, one should use the "Cahn–Hilliard-Reaction model", which includes thermodynamically consistent boundary conditions for molecules to enter and leave the pore space (Singh et al., 2008; Burch and Bazant, 2009). It is beyond the scope of this paper to analyze or simulate the intrapore adsorbate distribution in detail, but this would be interesting to pursue in future work. Such a nanoscale, statistical continuum model may be able to capture key features of molecular dynamics simulations (Gelb et al., 1999; Pellenq and Levitz, 2002; Coasne et al., 2007, 2008a, 2008b, 2009) at greatly reduced computational cost, thereby allowing extensions to experimental time and length scales.

4.2. Hierarchical wetting model

We proceed instead by making some simple approximations to enable us to predict general features of molecular condensation in nanoporous media. It is often reasonable to assume that in the first monolayer there are strong surface forces, which decay quickly with distance from the surface. In case of concrete, for example, water adsorption in C–S–H nanopores containing dissolved salts involves strong electrostatic forces, which are screened at the molecular scale due to diffuse charge, solvated ion crowding and electrostatic correlations (Pellenq et al., 1997; Bazant et al., 2011). For simplicity, let us assume that the regular solution model above describes the mean homogeneous coverage $\Omega_{hom}(h,T;c_T,\omega)$ of the first monolayer on the surface at low vapor pressure. Here, c_T and ω describe the local adsorption and interaction energies, which could depend on surface heterogeneities or curvature in very small pores. In thick pores at low vapor pressure, the dynamics of the concentration profile in the first monolayer could be described by the Allen–Cahn equation (Baluffi et al., 2005) for an open system (or its generalization for nonlinear adsorption kinetics Bai et al., 2011), since gas molecules are freely exchanged with the adsorbate at all points.

Here we consider what would happen in the general case of nanopores, which are thick enough to be covered by non-overlapping monolayers at low vapor pressure, but thin enough to be spanned by a condensed liquid phase at moderate vapor pressures (below the saturation pressure). Over experimental time scales (e.g. minutes to months), the Cahn–Hilliard equation predicts that small clusters of molecules or voids resulting from thermal fluctuations of the homogeneous state will coarsen within the nanopores, so as to minimize the gradient energy (which is the molecular analog of surface tension). Assuming strong wetting in the first monolayer, this coarsening proceeds until the size of the separated nanophases is set by the diameter of the bulk region just outside the first monolayer.

In that case, as a crude first approximation, we describe the bulk region by another regular solution model, whose characteristic lattice size is that of the pore bulk. The filling fraction of the bulk region is thus given by $\Theta_{hom}(h,T;c_T^b,\omega^b)$, where $c_T^b = \exp(\Delta g_a^b/k_B T)$ and ω^b are effective values for molecular droplets in the pore. The total weight of a homogeneous adsorbate in the pore is then given by

$$w_{hom}(h,T) = \Gamma_1 \Theta_{hom}(h,T;c_T,\omega) + \Gamma^b \Theta_{hom}(h,T;c_T^b,\omega^b) \tag{22}$$

where Γ_1 is the total weight of a full surface monolayer and Γ^b is the weight of the filled bulk region. This "Hierarchical Wetting" model is surely oversimplified, but it captures typical results of molecular dynamics simulations (Coasne et al., 2007, 2008a, 2008b, 2009) and allows considerable insight into experimental data, as we now explain.

4.3. Surface versus bulk phase separation in nanopores

This very simple model leads to two types of hysteresis, one due to the condensation of adatom clusters in the first monolayer at low vapor pressure and the second due to the condensation of pore-spanning clusters of molecules or voids ("nanodroplets" and "nanobubbles", respectively) in the bulk pore at higher vapor pressure. Each hysteresis has its own magnitude and critical temperature. If the pore radius is R and monolayer thickness, a, then the effective interaction parameter scales with the geometrical ratio:

$$\frac{\omega^b}{\omega} \approx \frac{T_c^b}{T_c} \approx \frac{\Delta h^b}{\Delta h} \approx \frac{R}{a} \tag{23}$$

which is typically larger than one, except in molecular scale pores (which might not be macroscopically accessible). An interesting implication is that critical temperature T_c^b for droplet phase separation in the bulk nanopore is larger from that of the first monolayer T_c by the same factor α. Well below the critical temperatures, the magnitude of the bulk hysteresis Δh^b (dominated by enthalpy) is also larger than that of the surface layer Δh, by the same factor. Bulk hysteresis is also shifted to larger humidities in the multilayer adsorption regime, assuming that the adsorption energy in the bulk is much less than it is at the surface, $\Delta g_a^b \ll \Delta g_a$.

These simple concepts are illustrated in Fig. 7. As the nanopore is emptied and filled, there are two instabilities corresponding to sudden phase separation in the first monolayer, at low vapor pressure, and in the bulk, at higher vapor pressure. The resulting desorption and sorption isotherms for this crude model already resemble the experimental data for concrete or cement paste at room temperature in Fig. 1. The theory also qualitatively predicts a nontrivial effect of temperature, which suppresses hysteresis in the monolayers at low vapor pressures more than in the bulk pores at higher vapor pressures.
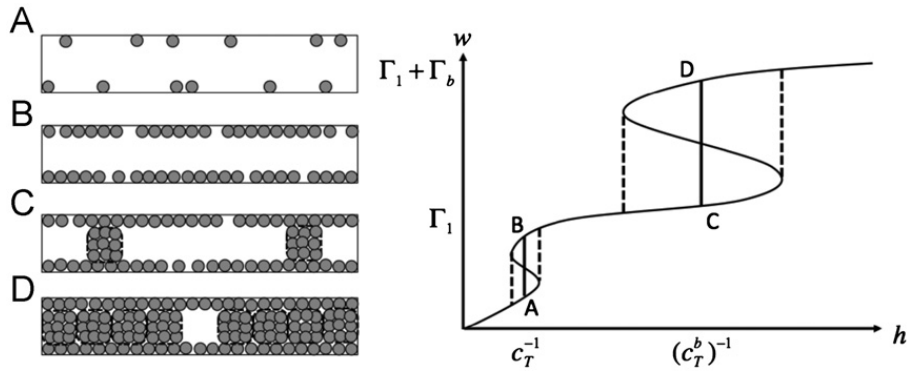
Fig. 7. Hierarchical wetting model for hindered multilayer adsorption in nanopores. The homogeneous isotherm, as in Eq. (22), exhibits two regions of hysteresis: (i) a small loop at low vapor pressure for low-density (A) and high-density (B) phases in the first monolayer and (ii) a larger loop at higher vapor pressure for the low-density (C) and high-density (D) phases of coarsened pore-spanning droplets and bubbles in the bulk fluid, outside the monolayer.

4.4. Snap-through instabilities

The reader may be wondering how our general statistical thermodynamic theory in Part II relates to the snap-through instabilities predicted for nonuniform pore openings in Part I. One major difference is that the theory of Part I does not account for the entropy of molecular rearrangements in the adsorbate and thus is mainly relevant for low temperature, where enthalpy dominates and sorption or desorption proceeds sequentially through the junction, like a crack tip. In the present model, phase separation can occur anywhere in the system that achieves a locally metastable state, and thus the sorption or desorption process can effectively tunnel through a junction. Nevertheless, a junction between two nanopores of different geometry or surface chemistry can act as a barrier for snap-through instabilities, due to the interfacial tension associated with lateral interactions across the junction.

To model the pinning effect of molecular interactions at junctions, we use again the Cahn–Hilliard (or Van der Waals) model (15), but it suffices to average over the cross section and focus on density gradients through the junction or pore opening. Relative to the free energy of an infinite system, the gradient energy per area (i.e. the interphasial tension at the junction) can be approximated as

$$\Delta G_i \approx \lambda K \left(\frac{\Delta \tilde{\Theta}}{\lambda}\right)^2 \approx \omega^b \Delta \tilde{\Theta}^2 \tag{24}$$

where λ is the local interface width and $\tilde{\Theta} = \Theta/\Theta_{max}$ is the jump in dimensionless adsorbate density, or total filling fraction ($0 < \tilde{\Theta} < 1$). This additional energy barrier must be overcome for phase separation to occur across the junction. Just as in the foregoing case of short pores, the interphasial tension can lead to hindrance or even suppression of phase separation.

When phase separation does occur across the junction, the chemical potential jumps according to Eq. (16) and causes an increase in humidity hysteresis at a given mean weight, due to the need to overcome the interfacial energy at the junction. As shown in Fig. 8 for the heterogeneous pore geometry in (a), this effect can be estimated graphically using Eq. (24) by plotting in (c) the two homogeneous isotherms as the dimensionless filling fraction $\tilde{\Theta}$ versus humidity h and measuring the density difference $\Delta \tilde{\Theta}$ between the two curves as the humidity is varied. The filling fraction jumps are also evident in the density profiles across heterogeneous pore in (d). The interfacial contribution to hysteresis at each junction, ΔG_i, which leads to the enlarged hysteresis in (d), can be of comparable magnitude to the intrinsic hysteresis for the interior of the pore, ω^b, since each results from the energy of lateral forces in a cross section of the pore. As the interfacial energy builds up during sorption, the humidity is gradually amplified by $\exp(\Delta G_i/k_B T)$, while during desorption the humidity is multiplied by $\exp(-\Delta G_i/k_B T)$. The net effect is to widen the hysteresis envelope associated with each phase separation process, e.g. in the first monolayer and the two types of bulk pores.

The sorption/desorption sequences predicted by these arguments using the simple Hierarchical Wetting Model are similar to those observed in molecular dynamics simulations of wetting fluids in heterogeneous nanopores by Coasne et al. (2007, 2008a, 2008b, 2009). The example shown in Fig. 8(a) consists of a series of multilayer-thick pores of two different radii a and b, which terminates at the free surfaces of much larger pores. The bulk regions of the thicker b pores have smaller adsorption energy Δg^b (larger c_T^{-1}) and larger interaction energy ω^b for spanning nanodroplets and nanobubbles than those of the thinner a pores. This leads to the different rescaled isotherms $\tilde{\Theta}(h)$ for a and b sections plotted in (c), which allow the sorption/desorption sequences to be predicted. During sorption starting from very low humidity, a monolayer first covers the entire pore surface in state A, and then bulk molecular condensation proceeds to the narrower sections in state B, followed by the thicker sections in state C. The corresponding spatial profiles of the filling fraction are shown in (d), from which the interfacial energies at the junctions can be estimated using Eq. (24). Due to the larger density jump at the pore ends, there is a larger interfacial energy there, compared to the internal a/b junctions, and this can cause condensation to occur in outermost pores after the others, leading to intermediate states B′ and C′ shown in (a).
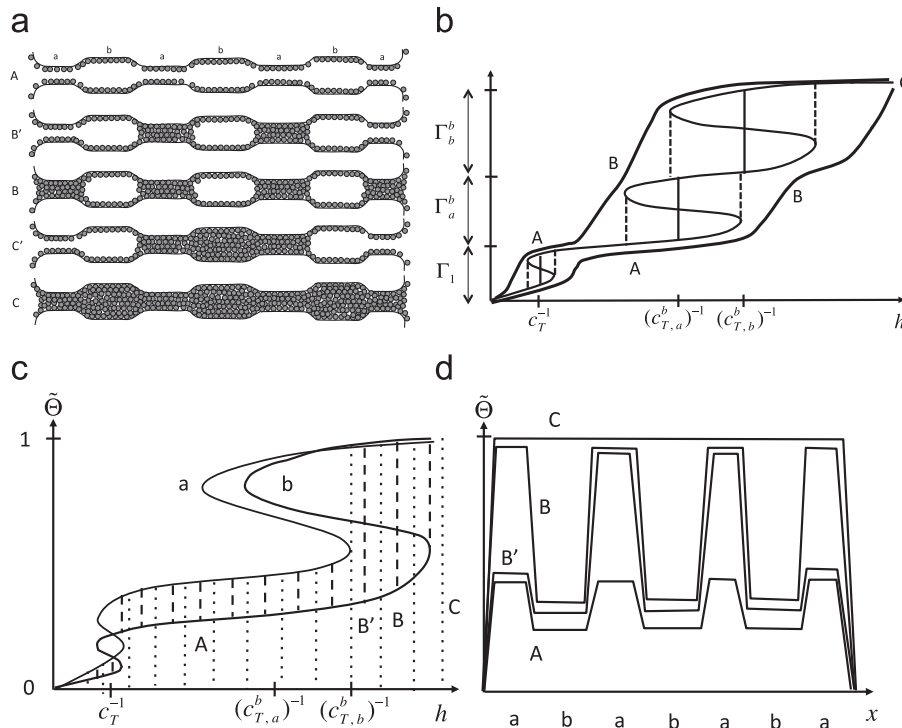
Fig. 8. Molecular condensation in a heterogeneous multilayer nanopore with sections *a* and *b* of two different thicknesses. (a) Typical molecular configurations A, B, B′, C, and C′ at different stages of sorption. (b) Net sorption and desorption isotherms for the nanopore including interfacial energies with the states A, B, and C indicated. (c) Isotherms of dimensionless filling fraction $\tilde{\Theta}$ (mean density) versus relative humidity *h* for the *a* and *b* sections of the pore, showing the jumps at *a/b* junctions (dashed lines) and the empty regions at the pore ends (dotted lines). (d) Spatial density profiles, $\tilde{\Theta}(x)$, for the states in part (a), where the interfacial energy due to each jump, which enhances the hysteresis in (b), scales as $\omega^b \Delta \tilde{\Theta}^2$.

4.5. Solid matrix deformation

Although we emphasize the statistical thermodynamic origin of sorption hysteresis, mechanical deformation of the solid matrix during phase separation could play an important role, even in the absence of pore collapse. Molecular condensation events lead to sudden changes in disjoining (or joining) pressure, which can influence neighboring pores, perhaps even triggering chains of subsequent phase separation events, as stresses are quickly transmitted through in the solid (at the local speed of sound). Analogous effects of "coherency strain" due to adsorption in elastic crystal lattices have recently been considered in Li-ion batteries and shown to contribute to suppression of phase separation and nonlinear pattern formation, consistent with experimental observations (Cogswell and Bazant, 2011). Ultimately, a complete model of sorption dynamics in nanoporous solids should take into account viscoelastic relaxation, or even plastic deformation and damage to the solid matrix, coupled to molecular condensation and transport.

5. Molecular condensation in nanoporous solids

5.1. Mosaic instability

It is important to emphasize that quasi-equilibrium phase separation across a nonuniform network of pores need not be sequential, as suggested in Part I based on mechanical analogies. As long as there is sufficient time for the chemical potential to equilibrate across the pore network between tiny, applied steps in humidity, then there is no prescribed order for the intermittent events of filling or emptying in different pores. At the macroscopic scale, the resulting "mosaic instability" of discrete molecular condensation events in different, tiny nanopores manifests itself by accumulating many incremental sorption/desorption isotherms into a smoother overall curve, as shown in Fig. 9. This effect has recently been invoked to explain the noisy thermodynamic hysteresis of voltage versus state of charge in phase-separating nanocomposite Li-ion battery cathodes (Dreyer et al., 2010, 2011).

This approximation inevitably breaks down, however, in sufficiently large porous bodies, where the transport of mass or heat is too slow to fully equilibrate the system between external humidity steps. In such cases, the progression of phase separation is biased by transport limitations and indeed behaves like a sequence of snap-through instabilities propagating through the porous medium, starting from the edges where the humidity is controlled. Analogous phenomena have also recently been predicted (Ferguson and Bazant, submitted for publication) and observed (Harris et al., 2010) in Li-ion batteries, where a narrow front of mosaic instability can propagate across the electrode from the separator, limited by diffusion of lithium ions in the electrolyte. Similar dynamical phase separation phenomena must occur during vapor sorption/desorption in porous media, but to our
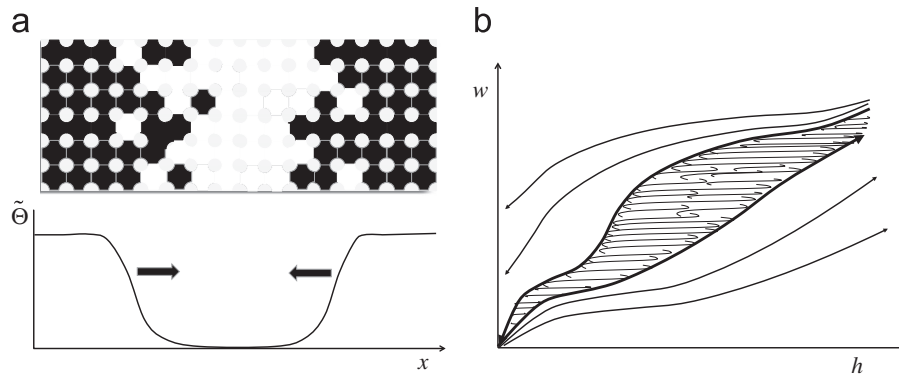
Fig. 9. Molecular condensation in macroscopic nanoporous solids. (a) Discrete nanopore transformations due to local mosaic instabilities propagate across the material in a narrow front from the edges where the vapor pressure is controlled. The front thickness scales with sweep rate dw/dt, and at high rates spans the system. (b) Sorption hysteresis due to quasi-equilibrium thermodynamics (thick solid lines) corresponding to countless, tiny condensation events (thin interior curves) for individual nanopores. With increasing sweep rate, there is additional non-thermodynamic hysteresis (thin exterior curves) due to internal resistances to transport and/or adsorption reaction kinetics.
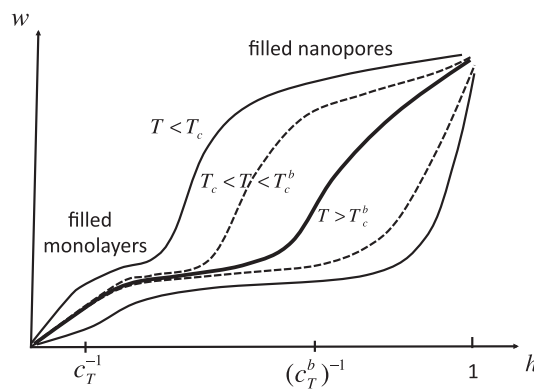

Fig. 10. Temperature dependence of sorption hysteresis in nanoporous solids with strong wetting. At low temperature, pronounced hysteresis exists at all vapor pressures (thin solid curves). Above the critical temperature T_c for phase separation in a monolayer, hysteresis disappears at low vapor pressure, but remains at high vapor pressure (dashed curves) until the critical temperature for bulk nanopore phase separation, T_c^b, is exceeded (thick solid curve).

knowledge no simple theory is yet available for the resulting macroscopic dynamics. Percolation concepts, which have been applied to sorption hysteresis due to classical capillarity in pore networks (Liu et al., 1993), may be useful, but molecular condensation, gas transport and adsorption reaction kinetics should also be considered. Analyzing the macroscopic dynamics of sorption and desorption in phase separating nanoporous solids would be a very interesting avenue for future research.

5.2. Rate dependence

Non-equilibrium phenomena always play a role in hysteresis, no matter how slowly experiment is performed. Whenever transport or adsorption kinetics are at least partly rate limiting, there will be an additional non-thermodynamic contribution to hysteresis, sketched in Fig. 9(b), which is related to the work done (or frictional energy dissipated) to drive the system, as noted in Part I. The faster the humidity sweep rate, the larger the hysteresis, in excess of the thermodynamic contribution described above. This effect is analogous to the "overpotential" or "internal resistances" observed in battery cycling under different conditions. For example, galvanostatic discharge is analogous to constant mass flux dw/dt, and more realistic situations for gas sorption, such as small humidity steps Δh or constant rate of humidity variation dh/dt, are analogous to potentiostatic intermittent titration and cyclic voltammetry, respectively. In principle, detailed mathematical modeling of transient vapor sorption/desorption taking into account transport, adsorption kinetics and phase separation could enable quantitative information about the material to be extracted from the rate-dependence of the observed hysteresis.

5.3. Temperature dependence

As noted above, the very simple Hierarchical Wetting Model already makes an interesting prediction about the temperature dependence of hysteresis in nanoporous solids with strong wetting. As sketched in Fig. 10, hysteresis is pronounced at low temperature and disappears at high temperature, but there is an intermediate range of temperatures ($T_c < T < T_c^b$) where hysteresis vanishes at low vapor pressure (monolayer filling) but persists at high vapor pressure (bulk nanopore filling). In complicated nanoporous geometries, the general effect should remain: As the temperature is increased, hysteresis vanishes first at low vapor pressure in the monolayer regime and then at high vapor pressure in the bulk nanopore regime. The reason is

that the effective interaction energy ω^b of pore-spanning nanodroplets and nanobubbles is larger than that of individual adsorbed molecules, due to the larger number of intermolecular bonds. Similar arguments apply to the interfacial energy ΔG_i at a nanopore junction, which is larger at high filling than for monolayer coverage. As a result, the critical hysteresis temperatures for different bulk nanopores are larger than for monolayers.

6. Re-interpretation of experimental data for concrete

As noted above, water sorption hysteresis at low humidity in concrete has long been attributed to pore collapse, in spite of the lack of any testable theory. It is noteworthy, therefore, that a number of puzzling experimental observations can be explained for the first time by molecular condensation without invoking any changes in the pore structure. In some cases, our predictions seem to be quantitatively consistent with the data, although more systematic experiments and detailed modeling should done, e.g. at different temperatures and humidity sweep rates, to further test the theory.

- *Inert gas versus water vapor*: No sorption hysteresis is observed for inert gases, such as nitrogen, in the same concrete samples that exhibit large hysteresis for water vapor (Baroghel-Bouny, 2007), and our model is able to attribute this effect to differences in lateral forces. Sorption experiments are usually carried out at room temperature, which is larger than the critical temperature T_c in our model (8), if the mean pair interaction energy ω is smaller than $2k_BT = 52$ meV. This is a reasonable upper bound for the weak lateral van der Waals forces in adsorbed inert gases, and so negligible hysteresis can be expected. In contrast, adsorbed water molecules have much stronger attractive forces, leading to room-temperature hysteresis, as explained next.
- *Hysteresis at low vapor pressure*: Our theory, although oversimplified, predicts hysteresis of a reasonable scale for monolayer water sorption at room temperature. Naively, we might estimate ω by the hydrogen bond enthalpy in bulk liquid water of 23.3 kJ/mol (Suresh and Naik, 2000), which would imply $T_c = 1380$ K, but this grossly overestimates the lateral pair interaction energy of adsorbed water molecules. A recent molecular dynamics study of water monolayers on hydrophilic silica surfaces has shown that 90% of the water molecules are "non-wetting", having much stronger bonds with the surface than with other water molecules (Romero-Vargas Castrillón et al., 2011). If we work backwards from our result in Fig. 5, then 1% hysteresis (in relative humidity) at room temperature implies $T_c = 410$ K or $\omega = 6.8$ kJ/mol, while 10% hysteresis implies $T_c = 660$ K or $\omega = 11$ kJ/mol. These are reasonable lateral interaction energies for adsorbed water molecules, which could quantitatively explain the observed hysteresis without any pore collapse.
- *Hysteresis at moderate vapor pressure*: In the regime of multilayer adsorption, we predict that the scale of hysteresis Δh^b is larger than in the monolayer regime Δh, very roughly scaling as the ratio of bulk pore radius to the monolayer thickness. This is consistent with the larger hysteresis that is always observed in the multilayer region (Baroghel-Bouny, 2007). It may even be possible to make quantitative connections with pore geometry, since the C–S–H pores and wetting layers in cement paste are indeed at the scale of 3–10 molecular diameters, as suggested by the hysteresis ratio.
- *Temperature dependence*: We predict that sorption hysteresis should decrease with increasing temperature, although we are not aware of any prior theoretical predictions or systematic experimental studies of this effect. In a recent study (Baroghel-Bouny, 2007), the hysteresis of water sorption in concrete at low vapor pressure (first monolayer) was negligible at 44 °C but quite significant at 23 °C, albeit in different concrete specimens, as shown in Fig. 1(a) and (b), respectively. The first adsorption isotherm was also steeper at 44 °C than at 23 °C (Figs. 3a and 9a of Baroghel-Bouny, 2007), suggesting that the free energy barriers responsible for hysteresis were lowered in the former case. Moreover, the curve of nearly reversible sorption/desorption at the higher temperature (Fig. 1(b)) passes roughly through the center of the hysteresis "window" between the first sorption and desorption curves (Fig. 1(a)) over a wide range of low humidities ($h < 60\%$). The data in Fig. 1(b) also makes the tantalizing suggestion of lingering hysteresis in the multilayer regime at an elevated temperature where hysteresis is already suppressed in the monolayer regime. This is consistent with our prediction that the critical temperature for condensation of larger droplets in nanopores is much larger than for individual adatoms in the first monolayer, as shown in Fig. 10.
- *Cycling history dependence*: Although we do not claim a quantitative understanding, it makes perfect sense in light of our theory that the first few sorption/desorption cycles often exhibit strong history dependence, where hysteresis grows with time, until a more reproducible path is achieved. This would naturally result from trapped condensed phases (droplets or bubbles) in the adsorbate, which may require nucleation to a larger perturbation to be released, e.g. from defects, cracks, or chemical heterogeneities. As explained above in the context of nanopore junctions, any heterogeneity can act as a pinning site for the adsorbate, effectively removing mass and increasing internal resistance during the initial sorption and desorption cycles. Of course, the same behavior is observed in rechargeable batteries, where the first few cycles are often very different from next hundred, e.g. due to the lithium trapping in interfacial films or defect sites, which lead to an irreversible initial capacity loss.

7. Conclusion

We have developed a simple thermodynamic theory of sorption/desorption hysteresis in nano porous solids, based on the concept of hindered molecular condensation. The model makes a number of novel and testable predictions that seem

consistent with previously unexplained data for cement paste and concrete, without postulating any pore collapse. Further experiments to systematically study the effects of temperature, humidity sweep rate, cycling behavior, etc., are proposed. The theory is very general and could be refined at the nanoscale and connected with macroscopic transport and mechanical deformation. The possibility of making quantitative predictions directly from the microstructure may lead to new, more accurate methods of determining the internal surface area and nanopore width distribution directly from the observed hysteresis of sorption and desorption isotherms. For concrete in particular, fruitful new directions for experiments suggested by our theory would involve systematically varying the temperature and humidity sweep rate during sorption/desorption of water vapor.

Acknowledgments

References

Adolphs, J., Setzer, M.J., Heine, P., 2002. Changes in pore structure and mercury contact angle of hardened cement paste depending on relative humidity. Mater. Struct. 35, 477–486.

Bai, P., Cogswell, D.A., Bazant, M.Z., 2011. Suppression of Phase Separation in LiFePO$_4$ Nanoparticles During Battery Discharge. preprint arXiv:1108.2326v1 [cond-mat.mtrl-sci].

Bazant, Martin Z., 2011. 10626 Electrochemical Energy Systems (Massachusetts Institute of Technology: MIT OpenCourseWare) ⟨http://ocw.mit.edu⟩ License: Creative Commons BY-NC-SA.

Bažant, Z.P., Bazant, M.Z. Theory of sorption hysteresis in nanoporous solids: I. Snap-through instabilities, http://dx.doi.org/10.1016/j.jmps.2012.04.014, this issue.

Bažant, Z.P., Cedolin, L., 1991. Stability of Structures: Elastic, Inelastic, Fracture and Damage Theories, Oxford University Press, New York (2nd ed., Dover Publ., 2003; 3rd ed., World Scientific Publishing, Singapore–New Jersey–London, 2010).

Bažant, Z.P., Kaplan, M.F., 1996. Concrete at High Temperatures: Material Properties and Mathematical Models. Longman (Addison-Wesley), London (monograph and reference volume, 412 + xii pp.; 2nd printing Pearson Education, Edinburgh, 2002).

Bažant, Z.P., Najjar, L.J., 1972. Nonlinear water diffusion in nonsaturated concrete. Mater. Struct. (RILEM, Paris) 5, 3–20. (reprinted in Fifty Years of Evolution of Science and Technology of Building Materials and Structures, Edited by F.H. Wittmann, RILEM, Aedificatio Publishers, Freiburg, Germany, 1997, pp. 435–456).

Baluffi, R., Allen, S.A., Carter, W.C., 2005. Kinetics of Materials. Wiley, New York.

Baroghel-Bouny, V., 2007. Water vapour sorption experiments on hardened cementitious materials part i: essential tool for analysis of hygral behaviour and its relation to pore structure. Cem. Concr. Res. 37, 414–437.

Bazant, M.Z., Storey, B.D., Kornyshev, A.A., 2011. Double layer in ionic liquids: overscreening versus crowding. Phys. Rev. Lett. 106, 046102.

Brunauer, S., 1943. The Adsorption of Gases and Vapors. Princeton University Press, Princeton NJ (p. 398).

Brunauer, S., Emmett, P.T., Teller, E., 1838. Adsorption of gases in multi-molecular layers. J. Am. Chem. Soc. 60, 309–319.

Burch, D., Bazant, M.Z., 2009. Size dependent spinodal and miscibility gaps in nanoparticles. Nano Lett. 9, 3795.

Cahn, J.W., 1961. On spinodal decomposition. Acta Metall. 9, 795–801.

Cahn, J.W., 1977. Critical point wetting. J. Chem. Phys. 66, 3667.

Cahn, J.W., Hilliard, J.E., 1958. Free energy of a nonuniform system. I. Interfacial energy. J. Chem. Phys. 28, 258.

Cerofolini, G.F., Meda, L., 1998a. A theory of multilayer adsorption on rough surfaces in terms of clustering and melting BET piles. Surf. Sci. 416, 402–432.

Cerofolini, G.F., Meda, L., 1998b. Clustering and melting in multilayer equilibrium adsorption. J. Colloid Interface Sci. 202, 104–123.

Coasne, B., Galarneua, A., Di Renzo, F., Pellenq, R.J.-M., 2007. Effect of morphological defects on gas adsorption in nano porous silicas. J. Phys. Chem. C 111, 15759–15770.

Coasne, B., Galarneau, A., Di Renzo, F., Pellenq, R.J.-M., 2008a. Molecular simulation of adsorption and intrusion in nanopores. Adsorption 14, 215–221.

Coasne, B., Di Renzo, F., Galarneau, A., Pellenq, R.J.-M., 2008b. Adsorption of simple fluid on silica surface and nanopore: effect of surface chemistry and pore shape. Langmuir 24, 7285–7293.

Coasne, B., Galarneau, A., Di Renzo, F., Pellenq, R.J.-M., 2009. Intrusion and retraction of fluids in nanopores: effect of morphological heterogeneity. J. Phys. Chem. C 113, 1953–1962.

Cohan, L.H., 1938. Sorption hysteresis and the vapor pressure of concave surfaces. J. Am. Chem. Soc. 60, 430–435.

Cogswell, D.A., Bazant, M.Z., 2012. Coherency strain and the kinetics of phase separation in LiFePO$_4$ nanoparticles. ACS Nano 6, 2215–2225.

Dreyer, D., Guhlke, C., Huth, R., 2011. The behavior of a many-particle electrode in a lithium-ion battery. Physica D 240, 1008–1019.

Dreyer, W., Jamnik, J., Guhlke, C., Huth, R., Moškon, J., Gaberšček, M., 2010. The thermodynamic origin of hysteresis in insertion batteries. Nat. Mater. 9, 448–451.

de Gennes, P.G., 1985. Wetting: statics and dynamics. Rev. Mod. Phys. 57, 827–863.

Espinosa, R.M., Franke, L., 2006. Influence of the age and drying process on pore structure and sorption isotherms of hardened cement paste. Cem. Concr. Res. 36, 1969–1984. (Figs. 2, 6, 16).

Feldman, R.F., Sereda, P.J., 1964. Sorption of water on compacts of bottle hydrated cement. I: the sorption and length-change isotherms. J. Appl. Chem. 14, 87.

Feldman, R.F., Sereda, P.J., 1968. A model for hydrated Portland cement paste as deduced from sorption-length change and mechanical properties. Mater. Struct. 1 (6), 509–520.

Ferguson, T.R., Bazant M.Z. Nonequilibrium thermodynamics of porous electrodes, submitted for publication, ⟨arXiv:1204.2934v1⟩ [physics.chem-ph].

Gelb, L.D., Gubbins, K.E., Radhakrishnan, R., Sliwinska-Bartkowiak, M., 1999. Phase separation in confined systems. Rep. Prog. Phys. 62, 1573–1659.

Gouin, H., 2009. Liquid nanofilms: a mechanical model for the disjoining pressure. Int. J. Eng. Sci. 47, 691–699.

Gouin, H., Gavrilyuk, S., 2008. Dynamics of liquid nanofilms. Int. J. Eng. Sci. 46, 1195–1202.

Guggenheim, E.A., 1952. Mixtures. Oxford University Press, London.

Harris, S.J., Timmons, A., Baker, D.R., Monroe, C., 2010. Direct *in situ* measurements of Li transport in Li-ion battery negative electrodes. Chem. Phys. Lett. 485, 265–274.

Hirth, J.P., Lothe, J., 1992. Theory of Dislocations. Kreiger.

Israelachvili, J., 1992. Intermolecular and Surface Forces. Academic Press, New York.

Jennings, H.M., Bullard, J.W., Thomas, J.J., Andrade, J.E., Chen, J.J., Scherer, G.W., 2008. Characterization and modeling of pores and surfaces in cement paste: correlations to processing and properties. J. Adv. Concr. Technol. 6 (1), 5–29.

Kang, B., Ceder, G., 2009. Battery materials for ultrafast charging and discharging. Nature 458, 190–193.

Liu, H., Zhang, L., Seaton, N.A., 1993. Analysis of sorption hysteresis in mesoporous solids using a pore network model. J. Colloid Interface Sci. 156, 285–293.

Malik, R., Burch, D., Bazant, M., Ceder, G., 2010. Particle size dependence of the ionic diffusivity. Nano Lett. 10, 4123–4127.

Malik, R., Zhou, F., Ceder, G., 2011. Kinetics of non-equilibrium lithium incorporation in $LiFePO_4$. Nat. Mater. 10 (8), 587–590.

Meethong, N., Huang, H.Y.S., Carter, W.C., Chiang, Y.M., 2007a. Size-dependent lithium miscibility gap in nanoscale $li_{1-x}FePO_4$. Electrochem. Solid-State Lett. 10, A134–A138.

Meethong, N., Huang, H.Y.S., Speakman, S.A., Carter, W.C., Chiang, Y.M., 2007b. Strain accommodation during phase transformations in olivine? based cathodes as a materials selection criterion for high? power rechargeable batteries. Adv. Funct. Mater. 17, 1115.

Nauman, E.B., Balsara, N.P., 1989. Phase equilibria and the Landau–Ginzburg functional. Fluid Phase Equilibria 45, 229–250.

Nauman, E.B., Rousar, I., Dutia, A., 1991. On the ultimate fineness of a dispersion. Chem. Eng. Commun. 105, 61–75.

Naumann, E.B., He, D.Q., 2001. Nonlinear diffusion and phase separation. Chem. Eng. Sci. 56, 1999–2018.

Nikitas, P., 1996. A simple statistical mechanical approach for studying multilayer adsorption: extensions of the BET adsorption isotherm. J. Phys. Chem. 100, 15247–15254.

Padhi, A.K., Nanjundaswamy, K.S., Goodenough, J.B., 1997. Phospho-olivines as positive-electrode materials for rechargeable lithium batteries. J. Electrochem. Soc. 144, 1188–1194.

Pellenq, R.J.-M., Levitz, P.E., 2002. Capillary condensation in a disordered mesoporous medium: a grand canonical Monte Carlo study. Mol. Phys. 100, 2059–2077.

Pellenq, R.J.-M., Caillol, J.M., Delville, A., 1997. Electrostatic attraction between two charged surfaces: a (N,V,T) monte carlo simulation. J. Phys. Chem. B 101, 8584–8594.

Powers, T.C., Brownyard, T.L., 1946. Studies of the physical properties of hardened portland cement paste. Part 2. Studies of water fixation. J. Am. Concr. Inst. 18 (3), 249–336.

Rarick, R.L., Bhatty, J.W., Jennings, H.M., 1995. Surface area measurement using gas sorption: application to cement paste. In: Skalny, J., Mindess, S. (Eds.), Material Science of Concrete IV, American Ceramic Society, pp. 1–41 (Chapter 1).

Romero-Vargas Castrillón, S., Giovambattista, N., Aksay, I.A., Debenedetti, P.G., 2011. Structure and energetics of thin film water. J. Phys. Chem. C 115, 4624–4635.

Rowlinson, J.S., Widom, B., 1984. Molecular Theory of Capillarity. Clarendon Press, Oxford.

Scherer, G.W., 1999. Structure and properties of gels. Cem. Concr. Res. 29, 1149–1157.

Seri-Levy, A., Avnir, D., 1993. The Brunauer–Emmett–Teller equation and the effects of lateral interactions: a simulation study. Langmuir 9, 2523–2529.

Singh, G.K., Ceder, G., Bazant, M.Z., 2008. Intercalation dynamics in rechargeable battery materials: general theory and phase transformation waves in $LiFePO_4$. Electrochim. Acta 53, 7599.

Suresh, S.J., Naik, V.M., 2000. Hydrogen bond thermodynamic properties of water from dielectric constant data. J. Chem. Phys. 113, 9727–9732.

Thomas, J.J., Allen, A.J., Jennings, H.M., 2008. Structural changes to the calcium hydrate gel phase of hydrated cement with age, drying and resaturation. J. Am. Ceram. Soc. 91 (10), 3362–3369.

Thornton, K., Ågren, J., Voorhees, P.W., 2003. Modelling the evolution of phase boundaries in solids at the meso- and nano-scales. Acta Mater. 51, 5675–5710.

van der Waals, J.D., 1893. The thermodynamic theory of capillarity under the hypothesis of a continuous variation of density (Translation by J. S. Rowlinson (1979)). J. Statist. Phys. 20, 197. (original version: Zeitscherift fuer Physikalische Chemie, Stoechiometrie und Verwandtschaftslehre, 13, 657).

Wagemaker, M., Singh, D.P., Borghols, W.J.H., Lafont, U., Haverkate, L., Peterson, V.K., Mulder, F.M., 2011. Dynamic solubility limits in nanosized olivine $LiFePO_4$. J. Am. Chem. Soc. 133, 10222–10228.

Widom, B., 1999. What do we know that van der Waals did not know? Physica A 263, 500–515.